TITLE

Geldanamycin-derived HSP90 Inhibitors are Synthetic Lethal with NRF2

AUTHORS

Liam Baird[1], Takafumi Suzuki[1], Yushi Takahashi[1], Eiji Hishinuma[2], Daisuke Saigusa[1,2], Masayuki Yamamoto[1,2]

AFFILIATIONS

[1]Department of Medical Biochemistry, Tohoku University Graduate School of Medicine, 2-1 Seiryo-machi, Aoba-ku, Sendai 980-8575, Japan

[2]Tohoku Medical Megabank Organization, Tohoku University, 2-1 Seiryo-machi, Aoba-ku, Sendai 980-8573, Japan

CORRESPONDENCE

liambaird@med.tohoku.ac.jp
masiyamamoto@med.tohoku.ac.jp

KEYWORDS

NRF2, KEAP1, oxidative stress, cancer, synthetic lethal

ABSTRACT

Activating mutations in KEAP1-NRF2 are frequently found in tumours of the lung, oesophageous and liver, where they are associated with aggressive growth, resistance to cancer therapies, and low overall survival. Despite the fact that NRF2 is a validated driver of tumorigenesis and chemotherapeutic resistance, there are currently no approved drugs which can inhibit its activity. Therefore, there is an urgent clinical need to identify NRF2-selective cancer therapies. To this end, we developed a novel synthetic lethal assay, based on fluorescently labelled isogenic wild-type and Keap1 knockout cell lines, in order to screen for compounds which selectively kill cells in an NRF2-dependent manner. Through this approach, we identified three compounds based on the geldanamycin scaffold which display synthetic lethality with NRF2. Mechanistically, we show that NRF2 target genes metabolize the quinone-containing geldanamycin compounds into more potent HSP90 inhibitors, which enhances their cytotoxicity while simultaneously restricting the synthetic lethal effect to cells with aberrant NRF2 activity. As all three of the geldanamycin-derived compounds have been used in clinical trials, they represent ideal candidates for drug repositioning to target the currently untreatable NRF2 activity in cancer.

INTRODUCTION

Pan-cancer genomic analyses have identified a multitude of signaling pathways which drive and sustain tumorigenesis (1). Unfortunately, in many cases the therapeutic exploitation of these validated cancer targets is limited by the lack of efficacious drugs which can specifically inhibit oncogenic signaling. For example, many tumour suppressors and oncogenic transcription factors lack deep, druggable binding pockets which makes the pharmaceutical manipulation of their activities particularly challenging (2). This inability to chemically modulate these bona fide cancer drivers presents a significant bottleneck in the fight against cancer.

One important oncogenic pathway whose activity cannot currently be inhibited by therapeutic interventions is the KEAP1-NRF2 pathway (1, 3, 4). Activating mutations in KEAP1-NRF2 signaling are present in 34% of squamous cell lung carcinoma, 22% of lung adenocarcinoma, 30% of oesophageal carcinoma, and 19% of hepatocellular carcinoma, and are associated with a poor prognosis and low overall survival (4-10). For example, in non-small cell lung carcinoma, patients with activating mutations in the NRF2 pathway have a mean overall survival of 11.2 months, compared with 36.8 months for tumours with intact NRF2 regulation (11). Thus, the high prevalence of aberrant NRF2 activation in tumours, coupled with a significant NRF2-dependent reduction in overall patient survival, means that there is considerable unmet clinical need for the development of NRF2-specific cancer therapies.

The transcription factor NRF2 regulates the cellular response to oxidative and electrophilic stresses through the upregulation of antioxidant and cytoprotective gene expression (12). Under non-stressed conditions, NRF2 is targeted for ubiquitination and proteasome-dependent degradation by its negative regulator KEAP1, which forms an E3 ubiquitin ligase with CUL3 and RBX1 (13, 14). In response to a wide range of cellular stresses, the KEAP1-dependent E3 ubiquitin ligase is inactivated, which results in the stabilization of NRF2, and a concomitant upregulation of the antioxidant transcription program (15-18).

During tumorigenesis, mutations which inactivate the KEAP1-dependent negative regulation of NRF2 result in the aberrant activation of the antioxidant transcription response. In this way, the cytoprotective functions of NRF2 are hijacked by the tumour,

conferring chemoresistance, tyrosine kinase inhibitor resistance and radiotherapy resistance upon the tumour cells, while simultaneously promoting cellular proliferation and metabolic rewiring (19-26). Together, these phenotypic changes contribute to the development of aggressive tumours with poor prognoses (9, 10, 22, 27). The oncogenic function of NRF2 has been validated in a variety of genetically engineered mouse models, which together confirm that, due to the central role that NRF2 plays in multiple important signaling nodes during tumour formation, survival and progression, it represents an excellent orphan drug target for novel cancer therapies (28, 29).

Current strategies for targeting NRF2-dependent tumours are primarily focused on the development of direct NRF2 inhibitors. These first-generation NRF2 inhibitors, including brusatol and halofuginone, are general protein translation inhibitors which do not exhibit specificity for the KEAP1-NRF2 pathway, and therefore have limited clinical potential (30, 31). As it is particularly challenging to develop drugs which directly inhibit the function of transcription factors like NRF2, we pursued a synthetic lethal strategy to specifically target NRF2-dependent tumours, as this obviates the need to identify direct NRF2 inhibitors. Because NRF2 regulates the expression of many drug metabolizing enzymes, it is an excellent candidate for synthetic lethal screening as its target genes may metabolize and activate prodrugs specifically in tumour cells with aberrant NRF2 activation. In the context of NRF2-dependent cancer, a synthetic lethal compound would only exhibit toxicity in cells with high levels of NRF2 activity, leaving the wild-type cells within the patient relatively insensitive to any harmful effects. This strategy provides a large therapeutic window for treatment, and allows for the development of compounds to target pathways often considered “non-druggable” (32).

In order to identify compounds which are synthetic lethal with NRF2, we developed a novel phenotypic screening strategy based on fluorescently labelled isogenic wild-type and Keap1 KO cell lines. The differential labelling of the cells allowed them to be mixed during the screen, as their genetic identity could be traced due to the differential fluorophore expression. During the post-screen data analysis, any compound which significantly altered the fluorophore ratio in favour of the wild-type cells would be considered a synthetic lethal hit.

In this study, we developed a novel synthetic lethal screening strategy to identify compounds which specifically kill cells with high levels of NRF2 activity. Through this

approach, we identified three compounds based on the geldanamycin scaffold, all of which have been through clinical trials, which are synthetic lethal with NRF2. Mechanistically, we show that NRF2 target genes effectively turn the geldanamycin-derived compounds into prodrugs which are selectively metabolized into more potent HSP90 inhibitors in cells with aberrant NRF2 activity. Together, our findings demonstrate that geldanamycin-based compounds represent excellent candidates for drug repositioning to target the currently undruggable KEAP1 and NRF2 mutations in human cancer.

RESULTS

Development and validation of a KEAP1-NRF2 synthetic lethal screening system

To identify compounds which are synthetic lethal with high levels of NRF2 activity, we developed a phenotypic screen based on an isogenic pair of fluorescently labelled Hepa1 cells (Fig 1A). CRISPR-Cas9 was used to knockout Keap1, resulting in the constitutive activation of Nrf2 and the upregulation of Nrf2-dependent target gene expression (Fig 1B) (33). Stable clones of the parental wild-type Hepa1 cells expressing EGFP, and Keap1 KO cells expressing mCherry, were generated, which allowed the genetic identity of the cells to be tracked throughout the screening process due to their differential fluorophore expression (Fig 1A). This enabled us to mix the WT-GFP and Keap1 KO-mCherry cells in the same microplate wells during the screen, guaranteeing that the cells experienced the same conditions when treated with the library of screening compounds, while simultaneously generating a greater dynamic range for the screening assay. Using this approach, any compound which could significantly decrease the ratio of mCherry:GFP would be considered a synthetic lethal hit (Fig 1A).

In monoculture conditions over a 5-day period, the fluorescence intensity from WT-GFP and Keap1 KO-mCherry cells plated at multiple densities increased with time, mirroring normal cell growth dynamics (Fig 1C, D). The increase in fluorescence intensity with time was comparable with the change in total protein content of the cultures, which supports the model that fluorescence intensity can be used as a metric for cell number (Fig 1E). Similarly, when co-cultured together, both the WT-GFP and Keap1 KO-mCherry cells displayed increased fluorescence intensity with time, with the Keap1 KO cells exhibiting enhanced proliferation, which is consistent with the positive role that Nrf2 plays in cell growth (Fig 1F)(23, 34). Visualisation of the co-culture of the WT-GFP and Keap1 KO-mCherry cells revealed uniform fluorophore expression between cells, further supporting the use of fluorescence intensity as a marker for cell survival during screening (Fig 1G).

Consistent with previous reports, treatment of the WT-GFP and Keap1 KO-mCherry co-cultured cells with the chemotherapeutic drugs doxorubicin or 5-FU resulted in the increased survival of the Keap1 KO cells relative to WT (Fig 1H, I)(19, 20). This highlights the cytoprotective role that Nrf2 activity plays in response to standard cancer therapies, while clearly demonstrating that the co-culture system accurately models the drug response

profile of NRF2-dependent tumours, and therefore is an appropriate model with which to screen for compounds which are synthetic lethal with NRF2 activity.

The HSP90 inhibitor 17-AAG is synthetic lethal with NRF2

NRF2 and its related factors regulate the physiological response to a wide variety of cellular stresses (34-36). As a result, cells with high levels of NRF2 activity are able to tolerate increased levels of oxidative stress, which may represent a shift in homeostasis relative to wild-type cells. As tumour cells are subject to a myriad of cellular stresses, we hypothesized that the NRF2-dependent change in one homeostatic set point may make the cells susceptible to orthogonal stressors (37-39). Therefore, as a pilot screen, we designed a chemical compound library to determine whether Keap1 KO cells display increased sensitivity to the modulation of ER stress, nutrient stress, oxidative stress, and proteotoxic stress response pathway activation. Any compound which reduced the mCherry: GFP ratio to a level less than three standard deviations below the DMSO control was considered to be a hit in the primary screen.

The induction of ER stress through the addition of tunicamycin or DTT, or oxidative stress through the addition of auranofin or BSO did not differentially impact the survival of WT or Keap1 KO cells, suggesting that activation of these stress response pathways is not synthetic lethal with Nrf2 activity (Fig 2A). Similarly, the induction of nutrient stress, through autophagy modulators (spermidine, chloroquine), mTORC inhibition (Torin 1) or SIRT1 deacetylase activity (resveratrol) did not result in increased toxicity in Keap1 KO cells (Fig 2A).

In contrast, we found induction of proteotoxic stress through the addition of the HSP90 inhibitor 17-AAG did result in Keap1 KO-specific toxicity at 100 nM, suggesting that this compound may be synthetic lethal with Nrf2 activity (Fig 2A). The fluorescence intensity-derived screening data were consistent with the visualization of the 17-AAG treated cells, as in response to 17-AAG treatment, the WT-GFP cells completely dominated the microplate well surface, suggesting that 17-AAG does not function to quench mCherry fluorescence, but instead directly impacts the survival of the Keap1 KO cells (Fig 2B). The determination of total protein content of WT and Keap1 KO cells in monoculture in response to 17-AAG provided complementary evidence, independent of fluorophore expression, that 17-AAG displays a synthetic lethal effect in Keap1 KO Hepa1 cells (Fig 2C).

Furthermore, 17-AAG treatment generates a wide therapeutic window in the nanomolar range in which it is toxic to Keap1 KO cells but not to the co-cultured WT cells (Fig 2D). The treatment of monocultures of WT or Keap1 KO cells provided a complementary result to the co-culture assay system, and showed that the synthetic lethal effect of 17-AAG in Keap1 KO cells is cell-intrinsic, and does not require communication between cells within the co-culture (Fig 2E, F).

To confirm that Nrf2 activity is required for this synthetic lethal phenotype, we generated a third isogenic cell line in which CRISPR-Cas9 was used to knockout Nrf2 in Keap1 KO-mCherry cells (DKO cells). The double knockout cells displayed a significant decrease in Nrf2 target gene expression (Fig 2G), but demonstrated normal growth dynamics (Fig 2H), albeit growing at a slower rate than the Keap1 KO cells. Importantly, in DKO cells the concomitant loss of Nrf2 expression completely rescued the synthetic lethal phenotype, unequivocally confirming that Nrf2 activity is required for 17-AAG's synthetic lethal effect (Fig 2I).

Time-course analysis using the co-culture system revealed that Keap1 KO-mCherry expression peaked at day 4, and then significantly decreased on days 5, 7 and 8, suggesting that the Keap1 KO cells were dying in response to 17-AAG, and not merely proliferating more slowly (Fig 2J). This phenotype was completely rescued in the co-culture of WT and DKO cells, further confirming the requirement of Nrf2 for the synthetic lethal effect (Fig 2K). Together, these data show that in isogenic Hepa1 cells, Nrf2 activity is necessary and sufficient for the synthetic lethal interaction with the HSP90 inhibitor 17-AAG.

17-AAG is synthetic lethal with NRF2 in human cancer cell lines

Activating mutations in the KEAP1-NRF2 pathway are common in tumours of the lung, oesophagus and liver (5-8). To confirm that the synthetic lethal relationship between Nrf2 and 17-AAG is not restricted to Hepa1 cells, we assayed ten human cancer cell lines, with differential levels of Nrf2 activation, derived from lung (A549, H2023, COR-L105, HCC827), oesophagus (KYSE70, KYSE30) and liver tumours (Huh-1, JHH5, Hep3B, JHH2). Furthermore, across these cell lines, NRF2 activation is achieved through a range of different mechanisms, which provides a more thorough understanding of the relationship between NRF2 activity and 17-AAG sensitivity: A549 cells contain an inactivating mutation in KEAP1 (G333C), KYSE70 cells have an oncogenic activating mutation in NRF2 (W24C), while

Huh-1 cells have high levels of phosphorylated p62, which drives constitutive NRF2 activation through a non-canonical pathway (19, 22, 24).

After long-term treatment with 17-AAG (8 days), all five cell lines with aberrant NRF2 activation showed significantly enhanced sensitivity to 17-AAG compared with the wild-type cells, which demonstrates that the synthetic lethal interaction between NRF2 and 17-AAG is not restricted to any single cell line or tissue type, but represents a ubiquitous interaction (Fig 3A, B). Within the lung and oesophageal cancer cell lines, A549 cells were significantly more sensitive to 17-AAG than all of the WT cell lines across the range of 100-800 nM, H2023 showed enhanced sensitivity from 50-800 nM, and KYSE70 cells displayed enhanced toxicity from 100-1,000 nM 17-AAG (Fig 3A). Within the liver cancer cell lines, Huh-1 cells showed significantly increased toxicity from 50-1,000 nM 17-AAG, while JHH5 cells were more sensitive than the WT liver cancer cell lines from 400-1,000 nM 17-AAG (Fig 3B). The same result was observed over a shorter treatment time-course of 4 days, which shows that the synthetic lethal interaction is a stable phenotype (Fig 3C). In this case, A549 cells displayed enhanced toxicity from 100-1,000 nM 17-AAG, KYSE70 from 50-800 nM, and Huh-1 cells were more sensitive than all of the WT cell lines from 50-1,000 nM 17-AAG (Fig 3C). Visualization of the cultures confirmed the enhanced 17-AAG-mediated cytotoxicity in cells with active KEAP1-NRF2 signaling (Fig 3D-H). Taken together, these data show that the synthetic lethal interaction between 17-AAG and NRF2 is a general phenomenon observed across all cell and tissue types.

Activation of NRF2 activity in wild-type cells enhances 17-AAG cytotoxicity

A salient feature of the KEAP1-NRF2 pathway is the inducibility of NRF2 activity, and concomitant upregulation of the antioxidant transcription program, in response to oxidative and electrophilic stresses (14). In order to determine whether NRF2 target genes are required for the synthetic lethal interaction with 17-AAG, we chemically induced the NRF2-dependent transcription response in human cancer cell lines which display normal regulation of the KEAP1-NRF2 pathway (Fig 3I, J). We found that co-treatment of cells with the NRF2 inducer DEM plus 17-AAG, resulted in significantly increased cytotoxicity when compared to treatment with 17-AAG alone. This result suggests that the activity of NRF2 target genes is required for the synthetic lethal effect of 17-AAG, and confirms that NRF2 activation is sufficient to confer enhanced 17-AAG cytotoxicity upon cells.

NRF2-dependent changes in HSP90, redox regulation or cellular proliferation are not required for the synthetic lethal phenotype

In order to gain an understanding of the molecular mechanism responsible for the synthetic lethal interaction between NRF2 and 17-AAG, we modulated each of NRF2's cellular functions in order to elucidate which, if any, are required for the synthetic lethal phenotype. As NRF2 is a transcription factor, and 17-AAG is an HSP90 inhibitor, we first addressed the possibility that an NRF2-dependent decrease in HSP90 gene expression may be responsible for the synthetic lethality, as a reduced cellular HSP90 chaperone pool would require lower levels of an inhibitor to induce toxicity. However, in isogenic Hepa1 cells, none of the four HSP90 homologues displayed reduced expression in response to constitutive Nrf2 activation, which shows that a reduction in the cellular HSP90 level is not responsible for the observed phenotype (Fig 4A).

As NRF2 is the master regulator of the cellular redox state, we next addressed whether 17-AAG may induce hyperactivation of NRF2, leading to supraphysiological levels of NRF2 activity, which may induce reductive stress-mediated cell death (40). However, in both WT and Keap1 KO cells, the NRF2 transcription program was not upregulated in response to 17-AAG treatment, which suggests that 17-AAG is not an NRF2 inducer (Fig 4B). To test whether supraphysiological levels of NRF2 alone can induce cell death, we knocked down β-TrCP in A549 cells, which lack KEAP1 activity due to the presence of an inactivating G333C mutation (Fig 4C). This siRNA treatment resulted in an increase in the NRF2 transcription response, even in the absence of functional KEAP1, through the suppression of the non-canonical GSK3-β-TrCP pathway of NRF2 degradation (41). This hyperactivated NRF2 state was not sufficient to induce cell death, while the addition of the antioxidant NAC also had no impact on the synthetic lethality of 17-AAG (Fig 4D,E). Together, these data show that NRF2's regulation of the cellular redox state is not required for the synthetic lethality with 17-AAG.

Active NRF2 signaling promotes rapid cellular proliferation, which is a hallmark of its oncogenic effect (23, 34). This enhanced proliferation may contribute to cell death if it reduces the cell cycle time below the level required to repair the cellular damage induced by the proteotoxic 17-AAG. To test this model, we reduced the cellular proliferation rate by culturing the isogenic Hepa1 cells in reduced serum media. However, while this resulted in a

significant decrease in cell proliferation, it had no impact on the synthetic lethality of 17-AAG, which argues against a role for NRF2-dependent enhanced proliferation in the synthetic lethal phenotype (Fig 4F). As NRF2-dependent changes to HSP90 levels, the cellular redox state, or cellular proliferation are not required for the synthetic lethality, these data suggest that the broader cell-wide phenotypic changes conferred by NRF2 activation are not required for increased 17-AAG sensitivity.

NRF2 is the main determinant of 17-AAG toxicity

To more clearly define the role of NRF2 in the synthetic lethal phenotype, we utilized the isogenic WT and DKO Hepa1 cells grown together in the co-culture system. Surprisingly, these co-culture assays revealed that the Nrf2-null DKO cells exhibit significantly less toxicity towards 17-AAG than the WT cells (Fig 4G, H). This strongly suggests that loss of Nrf2 is protective against 17-AAG, and therefore, that Nrf2 activity is the main factor in determining 17-AAG toxicity.

HSP90 inhibition by 17-AAG leads to the activation of the cytoprotective HSF1-dependent heat shock response (42, 43). In order to determine whether this HSP90-HSF1 axis is important for the NRF2 synthetic lethal phenotype, we carried out epistasis experiments using 17-AAG and the HSF1 inhibitor Kribb11. In WT cells, the inhibition of HSF1 coupled with 17-AAG treatment had no impact on cell survival, while in Keap1 KO cells, the co-treatment with Kribb11 resulted in increased cell death (Fig 4I). These data suggest that in Keap1 KO cells, 17-AAG induces cell death through the canonical HSP90-dependent proteostasis pathway, as the cell death can be further enhanced by inhibiting HSF1 only in Keap1 KO cells. Furthermore, analysis of cell membrane permeability conclusively showed that 17-AAG induces cell death, and not merely a reduction in cell proliferation, in an NRF2-dependent manner (Fig 4J). Taken together, these data show that the activity of NRF2 makes cells more sensitive to 17-AAG induced cell death through the canonical HSP90 inhibition pathway.

The geldanamycin scaffold is required for the synthetic lethal phenotype

As our data have shown that 17-AAG's function as an HSP90 inhibitor, and not cross-talk with one of the phenotypic changes induced by NRF2 activation, is required for the synthetic lethal phenotype, we assayed a broad range of HSP90 inhibitors to determine

whether HSP90 inhibition in general is synthetic lethal with NRF2. We selected five additional HSP90 inhibitors, based on a range of chemical scaffolds, to determine which, if any, are synthetic lethal with NRF2 (Fig 5A). In human lung cancer cell lines, we found that 17-DMAG, but not any of the other HSP90 inhibitors, displayed significantly enhanced toxicity specifically in the NRF2-active A549 cells (Fig 5B-F). Visually, while 50 nM 17-DMAG had no impact on the cell survival of COR-L105 cells, it resulted in significant cell death in the NRF2-active A549 cells (Fig 5G).

This result was confirmed in the isogenic Hepa1 cells, where synthetic lethality was also only observed with 17-DMAG, and not with the other HSP90 inhibitors (Fig 5H-K). As both 17-AAG and 17-DMAG are derived from the geldanamycin scaffold, these data suggest that within HSP90 inhibitors, only compounds derived from geldanamycin are synthetic lethal with NRF2. As both 17-AAG and 17-DMAG have been used in clinical trials to treat a range of different tumours, they represent excellent candidates for drug repositioning to target NRF2-dependent tumours (44-48).

Metabolism of the quinone in the geldanamycin-based compounds is responsible for the NRF2-specific synthetic lethality

To confirm the requirement of the geldanamycin scaffold for the synthetic lethal interaction, we tested a third geldanamycin-derived compound, IPI-504, which has also been used as a cancer treatment in clinical trials (49-51). In human lung and liver cancer-derived cell lines, as well as in the isogenic Hepa1 cells, IPI-504 displayed significantly enhanced toxicity in the A549, Huh-1 and Keap1 KO cells, which all display constitutive NRF2 activity (Fig 6A-F). Visualization of the IPI-504 treated cells confirmed that the compound is killing the cells is an NRF2-dependent manner (Fig 6B, D, F). Taken together, these results clearly demonstrate that amongst HSP90 inhibitors, the geldanamycin scaffold is an absolute requirement for synthetic lethality with NRF2.

The geldanamycin scaffold contains a quinone group which, in the case of 17-AAG, has been shown to be metabolized into a hydroquinone, 17-AAGH_2, which displays increased potency as an HSP90 inhibitor (Fig 7A)(52). To ascertain whether 17-AAG is metabolized into the more potent 17-AAGH_2 in an NRF2-dependent manner, we treated the isogenic WT and Keap1 KO Hepa1 cells with 17-AAG, and analysed the metabolites using LC-MS. Interestingly, we found that significantly more 17-AAGH_2 is produced in Keap1 KO than

WT cells, which strongly suggests that the metabolism of the quinone to the hydroquinone provides the mechanism for the NRF2-specific synthetic lethality of the geldanamycin-derived compounds (Fig 7B).

A number of NRF2 target genes have been shown to metabolize quinones, including NQO1 and TXNRD1, which are upregulated in NRF2-active human cancer cell lines (Fig 7C). As the metabolism of other quinone-containing compounds, like β-lapachone, has been used as an anti-cancer strategy, we investigated whether the synthetic lethal properties of the quinone-containing geldanamycin-derived compounds extend to other quinone drugs. Surprisingly, in human lung cancer cell lines, high levels of NRF2 provided enhanced survival in response to β-lapachone treatment (Fig 7D). These data strongly suggest that the synthetic lethal relationship between the geldanamycin-derived compounds and NRF2 does not represent a general susceptibility of NRF2 to all quinone-containing drugs.

In order to determine which NRF2 target gene is responsible for the metabolism of the quinone to the hydroquinone, we focused on two NRF2 target genes, NQO1 and TXNRD1, as their roles in quinone metabolism are well supported experimentally (52, 53). Small molecule inhibitors of NQO1 (dicoumarol), and TXNRD1 (auranofin) revealed an additive effect when inhibited together, which suggests that multiple NRF2 target genes can metabolize 17-AAG into the more potent 17-AAGH_2 (Fig 7E). To more clearly delineate the relative importance of NQO1 and TXNRD1 for the synthetic lethal interaction, we used CRISPR-Cas9 to knockout NQO1 in Huh-1 cells (Fig 7F). While addition of the TXNRD1 inhibitor auranofin induced a modest increase in cell survival in cells treated with 17-AAG, the genetic knockout of NQO1 almost completely rescued the lethality, suggesting that NQO1 is the main NRF2 target gene responsible for the metabolism of 17-AAG to the more potent 17-AAGH_2 (Fig 7G). Together, these data support a model whereby, in NRF2-dependent tumours, upregulation of antioxidant gene expression effectively turns the geldanamycin-derived HSP90 inhibitors into prodrugs which are metabolized into more potent compounds through the activity of the NRF2 target genes NQO1 and TXNRD1. This mechanism provides the specificity for the synthetic lethal interaction between NRF2 and 17-AAG, 17-DMAG and IPI-504.

17-AAG displays synthetic lethality with NRF2 in vivo

Chemotherapeutic drugs such as cisplatin have been shown to have no effect on tumour growth in xenotransplants using cells with active NRF2 signaling, presumably due to the cytoprotective activity which NRF2 confers on the tumour cells (31). To determine whether 17-AAG is able to inhibit NRF2-dependent tumours *in vivo*, we used a xenotransplantation model utilizing the Keap1 KO-mCherry cells, as this allowed us to accurately measure tumour growth *in situ* by using mCherry fluorescence imaged with IVIS (in vivo measuring system). We transplanted 2 $x10^6$ Keap1 KO cells subcutaneously into nude mice, and after an initial two-week growth period, treated them with 100 mg/kg of 17-AAG three times per week. After three weeks of treatment, we observed a significant decrease in tumour size in the mice treated with 17-AAG compared to the vehicle (Fig 8A, B), with no detrimental effects on overall mouse health as measured by body weight (Fig 8C). While the tumours in the vehicle treated mice increased in size by over 14-fold in the three-week treatment period, the tumours in the 17-AAG treated mice grew by less than 5-fold over the same time frame ($p < 0.05$). This provides strong evidence that 17-AAG is active towards NRF2-dependent tumours *in vivo*.

17-AAG displays enhanced toxicity in combination with AKT inhibition or paclitaxel

Large-scale genomic analyses have revealed that the most commonly co-mutated pathways in human tumours are KEAP1-NRF2 in combination with the PI3K-AKT pathway (1). As this is a clinically important sub-group of NRF2-dependent tumours, we wished to determine whether 17-AAG can enhance the anti-cancer cytotoxicity of AKT inhibition in an NRF2-dependent manner. In lung cancer cell lines, while KEAP1-deficient A549 cells show reduced sensitivity to AKT inhibition with MK-2206 compared to KEAP1-WT COR-L105 cells, co-treatment with 17-AAG specifically and significantly enhanced the toxicity of MK-2206 in A549 cells to a level below that of the KEAP1-WT cells (Fig 8D). Similarly, in liver cancer cell lines, the combination of 17-AAG and MK-2206 displays significantly enhanced toxicity in NRF2-activated Huh-1 cells when compared to Hep3B cells, which display basal NRF2 activity (Fig 8E). Furthermore, as 17-AAG has been used in combination with paclitaxel in clinical trials (44), we examined whether this drug combination also exhibits enhanced cytotoxicity in a NRF2-dependent manner. In the NRF2-activated Huh-1 cells, a fixed concentration of 17-AAG coupled with escalating concentration of paclitaxel was significantly more toxic than the single treatment of paclitaxel alone (Fig 8F). Importantly, in

405 Hep3B cells, the same drug combination showed no additive cytotoxic effects (Fig 8F).
406 Together, these data show that 17-AAG is suitable for use in combination therapies to
407 enhance the toxicity of complementary drugs in NRF2-dependent tumour cells.

DISCUSSION

Aberrant activation of NRF2 is a common event in human cancer. By hijacking NRF2's cytoprotective function, these tumours become highly resistant to a broad range of cancer therapies, and therefore have very poor prognoses. Furthermore, the lack of approved therapies to modulate NRF2's oncogenic functions means that there is a significant unmet clinical need to identify compounds which can specifically target NRF2 activity in tumours. Therefore, in this study we developed a novel synthetic lethal screening strategy with the aim of identifying compounds which specifically kill cells with high levels of NRF2 activity. Because NRF2 regulates the expression of a broad range of xenobiotic metabolizing enzymes, it is an ideal candidate for drug-based synthetic lethal screening, as its target genes may utilize the small compounds as bioactivatable prodrugs. This enzyme-dependent activation of the screening compounds would restrict the cytotoxicity to cells with aberrant NRF2 activity, and in doing so, generate a large therapeutic window for pharmaceutical intervention. Through this approach, we identified three geldanamycin-derived HSP90 inhibitors which all display synthetic lethality with NRF2.

By screening a custom library of cell stress pathway modulators in isogenic WT and Keap1 KO cells, we identified 17-AAG as candidate synthetic lethal compound with NRF2. This result, and pathway specificity, was confirmed through the use of Nrf2 KO cells and a range of human tumour-derived cells lines with both normal and aberrant NRF2 activation. Mechanistically, we found that the quinone-containing geldanamycin chemical scaffold was required for the synthetic lethal interaction, and in doing so, expanded the synthetic lethal compounds to include 17-AAG, 17-DMAG and IPI-504. Use of chemical inhibitors and CRISPR-knockout cells revealed that the activity of cytoprotective enzymes which are upregulated by NRF2 activation is required for the synthetic lethal phenotype.

Taken together, these data support the following model: aberrant activation of NRF2 in tumours results in the upregulation of the NRF2 antioxidant program, including the cytoprotective enzymes NQO1 and TXNRD1 (Fig 9). Upon treatment with geldanamycin-derived HSP90 inhibitors, NRF2 target genes effectively utilize these compounds as prodrugs, and, by metabolizing the quinones into hydroquinones, generate potent HSP90 inhibitors specifically in cells with oncogenic NRF2 activity, resulting in cell death. Thus, the

enhanced metabolic activation of the geldanamycin-derived prodrugs provides the mechanism for the specificity for the synthetic lethal interaction with NRF2.

Previously, a large-scale systematic screen focusing on the identification of novel genomic biomarkers for anti-cancer therapies found that the expression of four genes (NQO1, C5ORF14, CENTD3, LAMB2) correlated with increased sensitivity to 17-AAG (54). However, mutations in KEAP1 or NFE2L2 in relation to 17-AAG sensitivity were not identified using this approach. Similarly, analysis of exome sequencing from hepatocellular carcinoma allowed the authors to propose that tumours with high expression of NQO1 may be more sensitive to HSP90 inhibition (55). However, the presence of divergent mutation signatures across the cell lines makes it impossible to determine the requirement of NRF2 for this effect. Thus, to date, the specific role and requirement of NRF2 activation in the sensitivity to 17-AAG has not been investigated. As aberrant NRF2 activation results in reduced sensitivity to a myriad of anti-cancer therapies through a diverse range of mechanisms, it is not obvious *a priori* that activation of NRF2 alone would be sufficient to sensitize cells to 17-AAG. By using three isogenic cell lines (WT, Keap1 KO and Nrf2-Keap1 DKO), we were able to incontrovertibly determine the role of NRF2 in the sensitivity to geldanamycin-derived HSP90 inhibitors. As the KEAP1-NRF2 pathway functions as one of the central drivers of oncogenesis, it is important that unequivocal mechanistic support, and not merely correlative observations drawn from genome-scale studies, is provided so that the clinical relevance of this drug-biomarker pair can be clearly revealed.

The geldanamycin-derived HSP90 inhibitors which we have identified as being synthetic lethal with NRF2 have been utilized in both mono and combination therapies in clinical trials up to phase III for a range of tumour types, including multiple myeloma, non-small cell lung carcinoma, acute myeloid leukemia and gastrointestinal stromal tumours (44-48, 50, 51). This makes them ideal candidates for drug-repositioning as novel treatments for the orphan KEAP1-NRF2 pathway in cancer.

Of particular clinical interest is the application of these compounds for the treatment of non-small cell lung carcinoma, as activating mutations in the NRF2 pathway are found in 34% of squamous lung cell carcinoma, and 22% of lung adenocarcinoma, and in which activation of NRF2 correlates with a particularly poor prognosis (5, 6, 10). Importantly, we also found that in the context of NRF2-dependent cancer, 17-AAG toxicity can be further enhanced when used in combination with other drugs, such as inhibitors of AKT or HSF1

signaling. This suggests that in addition to use as a monotherapy, the geldanamycin-derived HSP90 inhibitors can also be used in combination therapies in which they may exhibit enhanced anti-tumour efficacy.

While 17-AAG, 17-DMAG and IPI-504 have all shown efficacy in clinical trials, to date, they have not been implemented in clinical practice for multiple reasons, including strength of intellectual property protection, time to commercialization, and hepatic toxicity associated with higher dose administration (44, 56, 57). In the case of the hepatic toxicity profile upon treatment with higher doses of IPI-504, the authors noted that, "if a cancer patient population were identified in which clinical benefit could be achieved, the observed profile might be acceptable with appropriate monitoring for, and management of, known toxicities" (57). We would advocate that patients with aggressive NRF2-dependent tumours may represent one such candidate patient population.

In summary, through a synthetic lethal screening approach, we have identified three candidate compounds for drug repositioning for the currently untreatable NRF2 activation in human cancer.

MATERIALS AND METHODS

Reagents

β-lapachone, MK-2206, Paclitaxel, BIIB021 and Kribb11 were purchased from Cayman Chemical (Ann Arbor, Michigan, USA). 17-AAG and PU-H71 was purchased from Selleck Chemicals (Houston, TX, USA). Radicicol was purchased from Focus Biomolecules (Pennsylvania, USA). 17-AAGH_2 was purchased from APExBIO (Houston, TX, USA). Doxorubicin was purchased from Sigma-Aldrich (Missouri, USA).Methanol and acetonitrile for LCMS were purchased from Kanto Chemical (Tokyo, Japan). Formic acid was purchased from FUJIFILM Wako Pure Chemical Corporation (Osaka, Japan). Purified water was obtained by a Milli-Q Gradient system (Millipore, Billerica, MA, USA).

Cell culture

All cells were maintained in high glucose Dulbecco's modified Eagle's medium (DMEM), except for the JHH2 and JHH5 cells, which were maintained William's E media, supplemented with 10% fetal bovine serum (FBS), and antibiotics. All cells were cultured in a humidified atmosphere with 5% CO_2 at 37°C.

Cell line generation

CRISPR-Cas9 was used to generate the clonal Keap1 KO Hepa1 cells (Ran et al. 2013). Briefly, the primers 5'-CACCGTGTGTCCTGCACGTGATGAA-3' and 5'-AAACTTCATCACGTGCAGGACACAC-3' were cloned into px549 (ver 2.0) to generate the targeting vector. This was transfected in Hepa1 cells using Lipofectamine 2000 (INVITROGEN). On the following day, the transfected cells were treated with puromycin for 24 hrs. The surviving cells were cultured for an additional seven days, before being plated at single cell densities into individual wells of 96-well plates. qPCR for enhanced Nrf2 target gene expression was used to determine the success of the Keap1 KO protocol. To generate the clonal Keap1 KO-mCherry and WT-GFP cell lines, pEGFP-C1 and pmCherry-C1 were transfected into WT and Keap1 KO Hepa1 cells, respectively. Two-weeks of G418 treatment was used to select for transfected cells, after which the surviving cells were plated at single cell densities into individual wells of 96-well plates. The optimum clones were selected based on brightness and uniformity of fluorophore expression. To generate the clonal

Keap1-Nrf2 DKO-mCherry cells, 5'-CACCGTTCATAGCAGAGCCCAGTGA-3' and 5'-AAACTCACTGGGCTCTGCTATGAAC were cloned into px549 (ver 2.0) to generate the targeting vector. This was transfected in Keap1 KO-mCherry cells using Lipofectamine 2000 (INVITROGEN). On the following day, the transfected cells were treated with puromycin for 24 hrs. The surviving cells were cultured for an additional seven days, before being plated at single cell densities into individual wells of 96-well plates. qPCR for reduced Nrf2 target gene expression was used to determine the success of the Nrf2 KO protocol. To generate the clonal Huh-1 NQO1 KO cells, 5'–CACCGTCGTACTGGCTCACTCAGAG-3' and 5'–AAACCTCTGAGTGAGCCAGTACGAC-3' were cloned into px549 (ver 2.0) to generate the targeting vector. This was transfected in Huh-1 cells using Lipofectamine 2000 (INVITROGEN). On the following day, the transfected cells were treated with puromycin for 7 days. The surviving cells were cultured for an additional seven days, before being plated at single cell densities into individual wells of 96-well plates. Immunoblot for NQO1 was used to determine the success of the NQO1 KO protocol

Screening conditions and fluorescence intensity calculations

For all experiments using co-cultured WT-GFP and Keap1 KO-mCherry cells, on "day -1" 1 $x10^3$ WT and 2 $x10^3$ Keap1 KO cells were mixed together in each individual well of a black 96-well plate (Corning #3904). On the following day (day 0), the compounds were added to the screening plates at the concentrations described in the text. Immediately after the addition of the compounds, the fluorescence intensities of GFP and mCherry were measured using a PHERAstar FS microplate reader (BMG Labtech, Ortenberg, Germany). The screening plates were then returned to the 37°C incubator until day 8, when the fluorescence intensity was measured again. The change in fluorescence for both GFP and mCherry during the growth period was calculated as "Day 8 – Day 0". The ratio of $mCherry_{Day\ 8\text{-}0}$: $GFP_{Day\ 8\text{-}0}$ was calculated by dividing the $mCherry_{Day\ 8\text{-}0}$ by $GFP_{Day\ 8\text{-}0}$. For a synthetic lethal compound, the numerator would decrease, while the denominator would be unchanged, and therefore overall the ratio of mCherry: GFP would decrease. Comparisons between treatments, or within different populations of GFP of mCherry cells were made by normalizing the data to the DMSO control. As the cell culture media contains a background fluorescence signal which is highest on Day 0, when the media is fresh, and decreases with time as the media components are metabolized by the cells, it is possible for

the Day 8 – Day 0 calculation to provide a negative value. For example, if a compound, such as IPI-504, efficiently kills the Keap1-mCherry cells, then no mCherry fluorescence signal will be generated, however the media background fluorescence will reduce with time as the WT-GFP cells metabolize the fluorescing culture media components. For the screen of the stress pathway modulators presented in Fig 2A, any $mCherry_{Day\ 8\text{-}0}$: $GFP_{Day\ 8\text{-}0}$ ratio which was more than three standard deviations below the ratio obtained for the DMSO treated wells was considered a hit. When using fluorescence intensity to determine the concentration-dependent effects of compounds such as 17-AAG on cell survival, the fluorescence intensity data for each fluorophore channel were normalized to the DMSO control. In such cases n = 6 for each concentration tested.

Cell survival assays for human cancer cells

On "day -1" 2 $x10^3$ cells were plated into each individual well of a 96-well plate. On the following day (day 0), the compounds were added to the screening plates at the concentrations described in the text. The 96-well plates were then incubated at 37^{o}C until day 8, when they were washed with PBS, and lysed with 25 µl RIPA buffer (50 mM Tris, 150 mM NaCl, 1% (v/v) NP-40, 0.5% (w/v) deoxycholic acid, 0.1% (w/v) SDS, pH7.4), after which they were frozen at -30^{o}C. Total protein concentrations for each well were determined using the BCA protein assay (Pierce) following the manufacturer's instructions, and were normalized to the DMSO controls for comparisons between and within cell types. In all cases, n = 6 for each concentration tested. Statistical comparisons were made between WT and mutant cell lines using a Student's T-Test.

Gene expression analysis by qPCR

Total RNA was prepared from cell lysates using TRIzol reagent (Life Technologies, Carlsbad, CA) in accordance with the manufacturer's instructions. A 1 µg aliquot of total RNA was reverse transcribed with ReverTra Ace (Toyobo, Osaka, Japan). The resultant cDNA was used as a temperate for quantitative reverse transcription-PCR (qRT-PCR) on a SYBR green 7300 real time PCR analyzer (Life Technologies). The primers used during the qPCR analysis are available upon request.

siRNA knockdown of βTrCP1/2

A549 cells were transfected with a single siRNA duplex which targeted both βTrCP1 and βTrCP2, using the oligos 5'GUGGAAUUUGUGGAACAUC-dTdT-3' and 3'-dTdT-CACCUUAAACACCUUGUAG-5' using Lipofectamine 2000 (INVITROGEN). The success of the knockdown was determined using qPCR for βTrCP1/2 and NRF2 target genes.

Cell death quantification

Cell death as determined by membrane permeabilization was determined using the CellTox assay (Promega), following the manufacturer's instructions. On "day -1" 2 x10^3 A549 or COR-L105 cells were plated to each well of black 96-well plate (Corning #3904). On day 0, 200 nM 17-AAG, along with the CellTox reagent, was added to the cells. On day 3, CellTox fluorescence was measured using a PHERAstar FS microplate reader (BMG Labtech, Ortenberg, Germany).

Tumor implantation experiments

Cell suspensions of Keap1 KO-mCherry Hepa1 cells (2 x10^6 cells in 100 µl PBS) were subcutaneously injected into the trunk of 5-week-old Balb/c-*nu*/*nu* female mice. 100 mg/kg of 17-AAG in 10% DMSO /90% corn oil, or vehicle alone, were intraperitoneally administered three times per week, for three weeks, starting 2 weeks after tumor implantation. Fluorescence intensity measurements from the implanted tumor were captured by an in vivo imaging system (IVIS) (PerkinElmer). All animals were housed in specific pathogen-free conditions, according to the regulations of *The Standards for Human Care and Use of Laboratory Animals of Tohoku University* and the *Guidelines for Proper Conduct of Animal Experiments* by the Ministry of Education, Culture, Sports, Science, and Technology of Japan.

17-AAG and 17-AAGH$_2$ analysis by UHPLC-MS/MS

Methanol (1 mL) was directly added to the cultured cells on a dish, and its lysate was obtained and transferred to a sample tube (15 mL). The sample was mixed for 30 sec and sonicated in an ultrasonic bath for 10 min. Then, the sample was centrifuged at 16,400 x g

for 20 min at 4°C. The supernatant (200 µL) was transferred to a sample vial and set on the autosampler. The sample (10 µL) was subjected to an ultra-high-performance liquid chromatography triple quadrupole mass spectrometry (UHPLC-MS/MS). The UHPLC-MS/MS analysis was performed on an UltiMate3000 system, which consist with the binary pumps, autosampler and column compartment (Thermo Fisher Scientific, San Jose, CA) interfaced to a TSQ Quantiva equipped with Heated-ESI operated in negative ion mode. The UHPLC separation was performed using a C18 column (CAPCELL PAK C18 ACR, 2.0 mm i.d. ×100 mm, 3 µm particle size; OSAKA SODA Co., Ltd. Osaka, Japan). The mobile phases were consisted of water containing 0.1% formic acid (A) and acetonitrile containing 0.1% formic acid (B). Analytes were separated by the gradient conditions; the initial condition was 0% B with 0.3 mL/min, followed by a linear gradient to 50% B from 3.0 min to 4.0 min, 90% B from 4.0 min to 6.1 min and 100% B from 6.1 min to 8.0 min. Then, the 100% B was maintained for 4.0 min; and the mobile phase was returned to the initial conditions and maintained for 3.0 min until the end of the run. The total run time was 15.0 min, and the temperature of column compartment was 40 °C. The spray voltage of HESI source, sheath gas, auxiliary gas, sweep gas, ion transfer tube temperature and vaporizer temperature were 2.5 kV, 40 arb, 15 arb, 2 arb, 350°C and 350°C, respectively. The sheath gas, auxiliary gas and sweep gas were nitrogen. 17-AAG and 17-AAGH$_2$ were analyzed in the selected reaction monitoring mode of the MS/MS system. The optimal precursor ion $[M+H]^+$, product ion $[M+H]^+$ and its collision energy were *m/z* 584.4, *m/z* 541.4 and 18 eV for 17-AAG, and *m/z* 586.4, *m/z* 543.3 and 17 eV for 17-AAGH$_2$. The collision gas was argon at a pressure of 1.5 mTorr. All the data was analyzed by Thermo Xcalibur 4.2.47 (Thermo Fisher Scientific, San Jose, CA, USA), and peak area of 17-AAG and 17-AAGH$_2$ detected at 6.3 min and 4.9 min on the chromatogram, respectively, were automatically calculated by the software and used for further data analytes.

ACKNOWLEDGEMENTS

We would like to thank all of the members of the Yamamoto lab for their thoughtful and stimulating discussions. This research was partially supported by the Platform Project for Supporting Drug Discovery and Life Science Research (Basis for Supporting Innovative Drug Discovery and Life Science Research (BINDS)) from AMED under Grant Number

645 JP17am0101001 (support number 1234), AMED-P-CREATE (JP19cm0106101 to MY), JSPS
646 KAKENHI 19H05649 (to M.Y.) and JSPS KAKENHI Grants-in-Aid for Early Career Scientists
647 19K16512 (to L.B.).

REFERENCES

1. Sanchez-Vega F, Mina M, Armenia J, Chatila WK, Luna A, La KC, Dimitriadoy S, Liu DL, Kantheti HS, Saghafinia S, Chakravarty D, Daian F, Gao Q, Bailey MH, Liang WW, Foltz SM, Shmulevich I, Ding L, Heins Z, Ochoa A, Gross B, Gao J, Zhang H, Kundra R, Kandoth C, Bahceci I, Dervishi L, Dogrusoz U, Zhou W, Shen H, Laird PW, Way GP, Greene CS, Liang H, Xiao Y, Wang C, Iavarone A, Berger AH, Bivona TG, Lazar AJ, Hammer GD, Giordano T, Kwong LN, McArthur G, Huang C, Tward AD, Frederick MJ, McCormick F, Meyerson M; Cancer Genome Atlas Research Network, Van Allen EM, Cherniack AD, Ciriello G, Sander C, Schultz N. 2018. Oncogenic Signaling Pathways in The Cancer Genome Atlas. Cell. 173(2):321-337.e10.

2. Lazo JS, Sharlow ER. 2016. Drugging Undruggable Molecular Cancer Targets. Annu Rev Pharmacol Toxicol. 56:23-40.

3. Padmanabhan B, Tong KI, Ohta T, Nakamura Y, Scharlock M, Ohtsuji M, Kang MI, Kobayashi A, Yokoyama S, Yamamoto M. 2006. Structural basis for defects of Keap1 activity provoked by its point mutations in lung cancer. Mol Cell. 21(5):689-700.

4. Shibata T, Ohta T, Tong KI, Kokubu A, Odogawa R, Tsuta K, Asamura H, Yamamoto M, Hirohashi S. 2008. Cancer related mutations in NRF2 impair its recognition by Keap1-Cul3 E3 ligase and promote malignancy. Proc Natl Acad Sci U S A. 105(36):13568-73.

5. Cancer Genome Atlas Research Network. 2012. Comprehensive Genomic Characterization of Squamous Cell Lung Cancers. Nature 489(7417):519-25.

6. Cancer Genome Atlas Research Network. 2014. Comprehensive Molecular Profiling of Lung Adenocarcinoma. Nature 511(7511):543-50.

7. Cancer Genome Atlas Research Network. 2017. Integrated Genomic Characterization of Oesophageal Carcinoma. Nature 541(7636):169-175.

8. Totoki Y, Tatsuno K, Covington KR, Ueda H, Creighton CJ, Kato M, Tsuji S, Donehower LA, Slagle BL, Nakamura H, Yamamoto S, Shinbrot E, Hama N, Lehmkuhl M, Hosoda F, Arai Y, Walker K, Dahdouli M, Gotoh K, Nagae G, Gingras MC, Muzny DM, Ojima H, Shimada K, Midorikawa Y, Goss JA, Cotton R, Hayashi A, Shibahara J, Ishikawa S, Guiteau J, Tanaka M, Urushidate T, Ohashi S, Okada N, Doddapaneni H, Wang M, Zhu Y, Dinh H, Okusaka T, Kokudo N, Kosuge T, Takayama T, Fukayama M, Gibbs RA, Wheeler DA, Aburatani H, Shibata T. 2014. Trans-ancestry Mutational Landscape of Hepatocellular Carcinoma Genomes. Nat Genet 46(12):1267-73.

9. Solis LM, Behrens C, Dong W, Suraokar M, Ozburn NC, Moran CA, Corvalan AH, Biswal S, Swisher SG, Bekele BN, Minna JD, Stewart DJ, Wistuba II. 2010. Nrf2 and Keap1 abnormalities in non-small cell lung carcinoma and association with clinicopathologic features. Clin Cancer Res. 16(14):3743-53.

694 10. Inoue D, Suzuki T, Mitsuishi Y, Miki Y, Suzuki S, Sugawara S, Watanabe M, Sakurada
695 A, Endo C, Uruno A, Sasano H, Nakagawa T, Satoh K, Tanaka N, Kubo H, Motohashi
696 H, Yamamoto M. 2012. Accumulation of p62/SQSTM1 is associated with poor prognosis in
697 patients with lung adenocarcinoma. Cancer Sci. 103(4):760-6.
698
699 11. Jeong Y, Hoang NT, Lovejoy A, Stehr H, Newman AM, Gentles AJ, Kong W, Truong
700 D, Martin S, Chaudhuri A, Heiser D, Zhou L, Say C, Carter JN, Hiniker SM, Loo BW Jr, West
701 RB, Beachy P, Alizadeh AA, Diehn M. 2017. Role of KEAP1/NRF2 and TP53 Mutations in Lung
702 Squamous Cell Carcinoma Development and Radiation Resistance. Cancer Discov. 7(1):86-
703 101.
704
705 12. Itoh K, Chiba T, Takahashi S, Ishii T, Igarashi K, Katoh Y, Oyake T, Hayashi N, Satoh K,
706 Hatayama I, Yamamoto M, Nabeshima Y., 1997. An Nrf2/small Maf heterodimer mediates
707 the induction of phase II detoxifying enzyme genes through antioxidant response elements.
708 Biochem Biophys Res Commun. 18;236(2):313-22.
709
710 13. Itoh K, Wakabayashi N, Katoh Y, Ishii T, Igarashi K, Engel JD, Yamamoto M., 1999. Keap1
711 represses nuclear activation of antioxidant responsive elements by Nrf2 through binding to
712 the amino-terminal Neh2 domain. Genes Dev. 13(1):76-86.
713
714 14. Baird L, Yamamoto M. 2020. The Molecular Mechanisms Regulating the KEAP1-NRF2
715 Pathway. Mol Cell Biol. 40(13):e00099-20.
716
717 15. Dinkova-Kostova AT, Holtzclaw WD, Cole RN, Itoh K, Wakabayashi N, Katoh Y, Yamamoto
718 M, Talalay P., 2002. Direct evidence that sulfhydryl groups of Keap1 are the sensors
719 regulating induction of phase 2 enzymes that protect against carcinogens and oxidants. Proc
720 Natl Acad Sci U S A. 99(18):11908-13.
721
722 16. Zhang DD, Hannink M., 2003. Distinct cysteine residues in Keap1 are required for Keap1-
723 dependent ubiquitination of Nrf2 and for stabilization of Nrf2 by chemopreventive agents
724 and oxidative stress. Mol Cell Biol. 23(22):8137-51.
725
726 17. McMahon M, Lamont DJ, Beattie KA, Hayes JD., 2010. Keap1 perceives stress via three
727 sensors for the endogenous signaling molecules nitric oxide, zinc, and alkenals. Proc Natl
728 Acad Sci U S A. 2010 107(44):18838-43.
729
730 18. Suzuki T, Muramatsu A, Saito R, Iso T, Adachi S, Kawaguchi S, Iwawaki T, Suda H, Morita
731 M, Baird L, Yamamoto M, 2019. Molecular Mechanism of Cellular Oxidative Stress Sensing
732 by Keap1. Cell Rep. 28(3):746-758.e4.
733
734 19. Singh A, Misra V, Thimmulappa RK, Lee H, Ames S, Hoque MO, Herman JG, Baylin
735 SB, Sidransky D, Gabrielson E, Brock MV, Biswal S. 2006. Dysfunctional KEAP1-
736 NRF2 interaction in non-small-cell lung cancer. PLoS Med. 3(10):e420.
737
738 20. Wang XJ, Sun Z, Villeneuve NF, Zhang S, Zhao F, Li Y, Chen W, Yi X, Zheng W, Wondrak
739 GT, Wong PK, Zhang DD. 2008. Nrf2 enhances resistance of cancer cells to
740 chemotherapeutic drugs, the dark side of Nrf2. Carcinogenesis. 29(6):1235-43.

741 21. DeNicola GM, Karreth FA, Humpton TJ, Gopinathan A, Wei C, Frese K, Mangal D, Yu
742 KH, Yeo CJ, Calhoun ES, Scrimieri F, Winter JM, Hruban RH, Iacobuzio-Donahue C, Kern
743 SE, Blair IA, Tuveson DA. 2011. Oncogene-induced Nrf2 transcription promotes ROS
744 detoxification and tumorigenesis. Nature. 475(7354):106-9.
745
746 22. Shibata T, Kokubu A, Saito S, Narisawa-Saito M, Sasaki H, Aoyagi K, Yoshimatsu
747 Y, Tachimori Y, Kushima R, Kiyono T, Yamamoto M. 2011. NRF2 mutation confers malignant
748 potential and resistance to chemoradiation therapy in advanced esophageal
749 squamous cancer. Neoplasia. 13(9):864-73.
750
751 23. Mitsuishi Y, Taguchi K, Kawatani Y, Shibata T, Nukiwa T, Aburatani H, Yamamoto M,
752 Motohashi H, 2012. Nrf2 redirects glucose and glutamine into anabolic pathways in
753 metabolic reprogramming. Cancer Cell. 2012 Jul 10;22(1):66-79.
754
755 24. Saito T, Ichimura Y, Taguchi K, Suzuki T, Mizushima T, Takagi K, Hirose Y, Nagahashi
756 M, Iso T, Fukutomi T, Ohishi M, Endo K, Uemura T, Nishito Y, Okuda S, Obata M, Kouno
757 T, Imamura R, Tada Y, Obata R, Yasuda D, Takahashi K, Fujimura T, Pi J, Lee MS, Ueno T, Ohe
758 T, Mashino T, Wakai T, Kojima H, Okabe T, Nagano T, Motohashi H, Waguri S, Soga
759 T, Yamamoto M, Tanaka K, Komatsu M. 2016. p62/Sqstm1 promotes malignancy of HCV-
760 positive hepatocellular carcinoma through Nrf2-dependent metabolic reprogramming. Nat
761 Commun. 7:12030.
762
763 25. Krall EB, Wang B, Munoz DM, Ilic N, Raghavan S, Niederst MJ, Yu K, Ruddy DA, Aguirre
764 AJ, Kim JW, Redig AJ, Gainor JF, Williams JA, Asara JM, Doench JG, Janne PA, Shaw
765 AT, McDonald Iii RE, Engelman JA, Stegmeier F, Schlabach MR, Hahn WC. 2017. KEAP1 loss
766 modulates sensitivity to kinase targeted therapy in lung cancer. Elife. 6. pii: e18970.
767
768 26. Hellyer JA, Stehr H, Das M, Padda SK, Ramchandran K, Neal JW, Diehn M, Wakelee HA.
769 2019. Impact of KEAP1/NFE2L2/CUL3 mutations on duration of response to EGFR tyrosine
770 kinase inhibitors in EGFR mutated non-small cell lung cancer. Lung Cancer. 134:42-45.
771
772 27. Zhang M, Zhang C, Zhang L, Yang Q, Zhou S, Wen Q, Wang J. 2015. Nrf2 is
773 a potential prognostic marker and promotes proliferation and invasion in human
774 hepatocellular carcinoma. BMC Cancer. 15:531.
775
776 28. Romero R, Sayin VI, Davidson SM, Bauer MR, Singh SX, LeBoeuf SE, Karakousi TR, Ellis
777 DC, Bhutkar A, Sánchez-Rivera FJ, Subbaraj L, Martinez B, Bronson RT, Prigge JR, Schmidt
778 EE, Thomas CJ, Goparaju C, Davies A, Dolgalev I, Heguy A, Allaj V, Poirier JT, Moreira
779 AL, Rudin CM, Pass HI, Vander Heiden MG, Jacks T, Papagiannakopoulos T. 2017. Keap1 loss
780 promotes Kras-driven lung cancer and results in dependence on glutaminolysis. Nat
781 Med. 23(11):1362-1368.
782
783 29. Best SA, De Souza DP, Kersbergen A, Policheni AN, Dayalan S, Tull D, Rathi V, Gray
784 DH, Ritchie ME, McConville MJ, Sutherland KD. 2018. Synergy between the KEAP1/NRF2 and
785 PI3K Pathways Drives Non-Small-Cell Lung Cancer with an Altered Immune
786 Microenvironment. Cell Metab. 27(4):935-943.e4.
787

30. Ren D, Villeneuve NF, Jiang T, Wu T, Lau A, Toppin HA, Zhang DD. 2011. Brusatol enhances the efficacy of chemotherapy by inhibiting the Nrf2-mediated defense mechanism. Proc Natl Acad Sci U S A. 108(4):1433-8.

31. Tsuchida K, Tsujita T, Hayashi M, Ojima A, Keleku-Lukwete N, Katsuoka F, Otsuki A, Kikuchi H, Oshima Y, Suzuki M, Yamamoto M. 2017. Halofuginone enhances the chemo-sensitivity of cancer cells by suppressing NRF2 accumulation. Free Radic Biol Med. 103:236-247.

32. O'Neil NJ, Bailey ML, Hieter P. 2017. Synthetic lethality and cancer. Nat Rev Genet. 18(10):613-623.

33. Ran FA, Hsu PD, Wright J, Agarwala V, Scott DA, Zhang F. 2013. Genome engineering using the CRISPR-Cas9 system. Nat Protoc. 8(11):2281-2308.

34. Malhotra D, Portales-Casamar E, Singh A, Srivastava S, Arenillas D, Happel C, Shyr C, Wakabayashi N, Kensler TW, Wasserman WW, Biswal S., 2010. Global mapping of binding sites for Nrf2 identifies novel targets in cell survival response through ChIP-Seq profiling and network analysis. Nucleic Acids Res. 38(17):5718-34.

35. Glover-Cutter KM, Lin S, Blackwell TK. 2013. Integration of the unfolded protein and oxidative stress responses through SKN-1/Nrf. PLoS Genet. 9(9):e1003701.

36. Baird L, Tsujita T, Kobayashi EH, Funayama R, Nagashima T, Nakayama K, Yamamoto M, 2017. A Homeostatic Shift Facilitates Endoplasmic Reticulum Proteostasis through Transcriptional Integration of Proteostatic Stress Response Pathways. Mol Cell Biol. 2017 Feb 1;37(4). pii: e00439-16.

37. Gorrini C, Harris IS, Mak TW. 2013. Modulation of oxidative stress as an anticancer strategy. Nat Rev Drug Discov. 12(12):931-47.

38. Wang M, Kaufman RJ. 2014. The impact of the endoplasmic reticulum protein-folding environment on cancer development. Nat Rev Cancer. 14(9):581-97.

39. Levy JMM, Towers CG, Thorburn A. 2017. Targeting autophagy in cancer. Nat Rev Cancer. 17(9):528-542.

40. Rajasekaran NS, Connell P, Christians ES, Yan LJ, Taylor RP, Orosz A, Zhang XQ, Stevenson TJ, Peshock RM, Leopold JA, Barry WH, Loscalzo J, Odelberg SJ, Benjamin IJ. 2007. Human alpha B-crystallin mutation causes oxido-reductive stress and protein aggregation cardiomyopathy in mice. Cell. 130(3):427-39.

41. Rada P, Rojo AI, Chowdhry S, McMahon M, Hayes JD, Cuadrado A. 2011. SCF β-TrCP promotes glycogen synthase kinase 3-dependent degradation of the Nrf2 transcription factor in a Keap1-independent manner. Mol Cell Biol. 31(6):1121-33.

834 42. Zou J, Guo Y, Guettouche T, Smith DF, Voellmy R. 1998. Repression of heat shock
835 transcription factor HSF1 activation by HSP90 (HSP90 complex) that forms a stress-sensitive
836 complex with HSF1. Cell. 94(4):471-80.
837
838 43. Goetz MP, Toft D, Reid J, Ames M, Stensgard B, Safgren S, Adjei AA, Sloan J, Atherton
839 P, Vasile V, Salazaar S, Adjei A, Croghan G, Erlichman C. 2005. Phase I trial of 17-allylamino-
840 17-demethoxygeldanamycin in patients with advanced cancer. J Clin Oncol. 23(6):1078-87.
841
842 44. Jhaveri K, Taldone T, Modi S, Chiosis G. 2012a. Advances in the clinical development
843 of heat shock protein 90 (Hsp90) inhibitors in cancers. Biochim Biophys Acta. 1823(3):742-
844 55.
845
846 45. Richardson PG, Badros AZ, Jagannath S, Tarantolo S, Wolf JL, Albitar M, Berman
847 D, Messina M, Anderson KC. 2010. Tanespimycin with bortezomib: activity in
848 relapsed/refractory patients with multiple myeloma. Br J Haematol. 150(4):428-37.
849
850 46. Richardson PG, Chanan-Khan AA, Lonial S, Krishnan AY, Carroll MP, Alsina M, Albitar
851 M, Berman D, Messina M, Anderson KC. 2011. Tanespimycin and bortezomib combination
852 treatment in patients with relapsed or relapsed and refractory multiple myeloma: results of
853 a phase 1/2 study. Br J Haematol. 153(6):729-40.
854
855 47. Lancet JE, Gojo I, Burton M, Quinn M, Tighe SM, Kersey K, Zhong Z, Albitar MX, Bhalla
856 K, Hannah AL, Baer MR. 2010. Phase I study of the heat shock protein 90 inhibitor
857 alvespimycin (KOS-1022, 17-DMAG) administered intravenously twice weekly to patients
858 with acute myeloid leukemia. Leukemia. 24(4):699-705.
859
860 48. Jhaveri K, Miller K, Rosen L, Schneider B, Chap L, Hannah A, Zhong Z, Ma W, Hudis
861 C, Modi S. 2012b. A phase I dose-escalation trial of trastuzumab and alvespimycin
862 hydrochloride (KOS-1022; 17 DMAG) in the treatment of advanced solid tumors. Clin Cancer
863 Res. 18(18):5090-8.
864
865 49. Sydor JR, Normant E, Pien CS, Porter JR, Ge J, Grenier L, Pak RH, Ali JA, Dembski
866 MS, Hudak J, Patterson J, Penders C, Pink M, Read MA, Sang J, Woodward C, Zhang
867 Y, Grayzel DS, Wright J, Barrett JA, Palombella VJ, Adams J, Tong JK. 2006. Development of
868 17-allylamino-17-demethoxygeldanamycin hydroquinone hydrochloride (IPI-504), an anti-
869 cancer agent directed against Hsp90. Proc Natl Acad Sci U S A. 103(46):17408-13.
870
871 50. Sequist LV, Gettinger S, Senzer NN, Martins RG, Jänne PA, Lilenbaum R, Gray JE, Iafrate
872 AJ, Katayama R, Hafeez N, Sweeney J, Walker JR, Fritz C, Ross RW, Grayzel D, Engelman
873 JA, Borger DR, Paez G, Natale R. 2010. Activity of IPI-504, a novel heat-shock protein 90
874 inhibitor, in patients with molecularly defined non-small-cell lung cancer. J Clin
875 Oncol. 28(33):4953-60.
876
877 51. Wagner AJ, Chugh R, Rosen LS, Morgan JA, George S, Gordon M, Dunbar J, Normant
878 E, Grayzel D, Demetri GD. 2013. A phase I study of the HSP90 inhibitor retaspimycin
879 hydrochloride (IPI-504) in patients with gastrointestinal stromal tumors or soft-tissue
880 sarcomas. Clin Cancer Res.19(21):6020-9.

881
882
883 52. Guo W, Reigan P, Siegel D, Zirrolli J, Gustafson D, Ross D. 2005. Formation of 17-
884 allylamino-demethoxygeldanamycin (17-AAG) hydroquinone by NAD(P)H:quinone
885 oxidoreductase 1: role of 17-AAG hydroquinone in heat shock protein 90 inhibition. Cancer
886 Res. 65(21):10006-15.
887
888 53. Cenas N, Nivinskas H, Anusevicius Z, Sarlauskas J, Lederer F, Arnér ES. 2004. Interactions
889 of quinones with thioredoxin reductase: a challenge to the antioxidant role of the
890 mammalian selenoprotein. J Biol Chem. 279(4):2583-92.
891
892 54. Garnett MJ, Edelman EJ, Heidorn SJ, Greenman CD, Dastur A, et al. 2012. Systematic
893 identification of genomic markers of drug sensitivity in cancer cells. Nature 483(7391):570-5.
894
895 55. Schulze K, Imbeaud S, Letouzé E, Alexandrov LB, Calderaro J et al. 2015. Exome
896 sequencing of hepatocellular carcinomas identifies new mutational signatures and potential
897 therapeutic targets. Nat Genet 47(5):505-511.
898
899 56. Wang H, Lu M, Yao M, Zhu W. 2016. Effects of treatment with an Hsp90 inhibitor in
900 tumors based on 15 phase II clinical trials. Mol Clin Oncol 5(3):326-334.
901
902 57. Oh WK, Galsky MD, Stadler WM, Srinivas S, Chu F, Bubley G, Goddard J, Dunbar J, Ross
903 RW. 2011. Multicenter phase II trial of the heat shock protein 90 inhibitor, retaspimycin
904 hydrochloride (IPI-504), in patients with castration-resistant prostate cancer. Urology
905 78(3):626-30.

FIGURE LEGENDS

Fig. 1 | Development of an assay to identify compounds which are synthetic lethal with Nrf2.

A, Scheme showing an overview of the synthetic lethal screening strategy using isogenic WT and Keap1 KO Hepa1 cells. **B,** Nrf2 target genes are significantly upregulated in the CRISPR-Cas9 generated Keap1 KO Hepa1 cells, when compared to the parental WT cells. **C,** WT-GFP cells plated at multiple densities display normal growth dynamics over a five-day period. **D,** Keap1 KO-mCherry cells plated at multiple densities display normal growth dynamics over a five-day period. **E,** When co-cultured together at an initial seeding of 1,000 WT-GFP cells and 2,000 Keap1 KO-mCherry cells, both cell lines proliferate together at an expected rate over an 8-day period. **F,** Over a 4-day period, the fluorescence intensity of the WT-GFP and Keap1 KO-mCherry monocultured cells increases at a comparable rate to the increase in total protein content. **G,** Visualization of the co-culture of WT-GFP and Keap1 KO-mCherry cells, showing uniform fluorophore expression between the cells. Scale bar = 300 µm. **H, I,** Under co-culture conditions, when compared to the Keap1 KO-mCherry cells (orange line), the WT-GFP cells (blue line) are significantly more sensitive to the anticancer drugs 5-FU and doxorubicin.

Fig. 2 | The HSP90 inhibitor 17-AAG is synthetic lethal with Nrf2.

A, A screen of a library of stress pathway modulators reveals that the proteotoxic HSP90 inhibitor 17-AAG is synthetic lethal with Nrf2 activity in Hepa1 cells. **B,** Visualization of the co-cultured WT-GFP and Keap1 KO-mCherry cells shows that in response to DMSO, the co-culture is dominated by mCherry expressing cells, while in 17-AAG treated cells, the mCherry signal is significantly diminished, and the GFP expressing cells expand their domain to fill the entire surface of the microplate well. Scale bar = 300 µm. **C,** Validation of the fluorescence-based primary screen using total protein content as a measure of cell survival. Keap1-KO cells show significantly enhanced sensitivity to 17-AAG at 50 and 100 nM, which is independent of the measurement of fluorescence intensity. * $p < 0.05$. **D,** Viabilities of co-cultured WT-GFP (blue line) and Keap1 KO-mCherry cells (orange line), determined by fluorescence intensity relative to the DMSO control, exposed to the indicated concentrations of 17-AAG for 8 days.

E, Fluorescence intensity of WT-GFP cells exposed to 0.1% DMSO or 100 nM 17-AAG, measured each day over a period of 8 days. **F,** Fluorescence intensity of Keap1 KO-mCherry cells exposed to 0.1% DMSO or 100 nM 17-AAG, measured each day over a period of 8 days. **G,** Nrf2 target genes are significantly downregulated in the CRISPR-Cas9 generated Keap1-Nrf2 DKO Hepa1 cells, when compared to the parental Keap1 KO-mCherry cells. **H,** Keap1-Nrf2 DKO-mCherry cells plated at multiple densities display normal growth dynamics over a five-day period. **I,** Fluorescence intensity of Keap1-Nrf2 DKO-mCherry cells exposed to 0.1% DMSO or 100 nM 17-AAG, measured each day over a period of 8 days. **J,** Viabilities of co-cultured WT-GFP and Keap1 KO-mCherry cells, determined by fluorescence intensity, exposed to 0.1% DMSO or 100 nM 17-AAG, measured each day over a period of 8 days. The Keap1 KO data are depicted with the dashed line, while the WT cell data are shown with the unbroken line. * $p < 0.05$. **K,** Viabilities of co-cultured WT-GFP and Keap1-Nrf2 DKO-mCherry cells, determined by fluorescence intensity, exposed to 0.1% DMSO or 100 nM 17-AAG, measured each day over a period of 8 days.

Fig. 3 | 17-AAG is synthetic lethal with NRF2 in a range of different human cancer cell lines.

A, Viabilities of mono-cultured NRF2-active A549, H2023 and KYSE70 cells, and NRF2-normal COR-L105, HCC827 and KYSE30 cells. Cell viabilities were determined by total protein content, after exposure to the indicated concentrations of 17-AAG for 8 days. For a given concentration of 17-AAG, the NRF2-active cell lines were designated as sensitive to 17-AAG if their survival was statistically significantly reduced compared to all of the WT cells. **B,** Viabilities of mono-cultured liver cancer cell lines. Cell viabilities of NRF2-active Huh-1 and JHH5 cells, and NRF2-normal Hep3B and JHH2 cells, were determined by total protein content, after exposure to the indicated concentrations of 17-AAG for 8 days. For a given concentration of 17-AAG, the NRF2-active cell lines were designated as sensitive to 17-AAG if their survival was statistically significantly reduced compared to all of the WT cells. **C,** Viabilities of mono-cultured NRF2-active A549, KYSE70 and Huh-1 cells, and NRF2-normal COR-L105, KYSE30 and Hep3B cells. Cell viabilities were determined by total protein content, after exposure to the indicated concentrations of 17-AAG for 4 days. For a given concentration of 17-AAG, the NRF2-active cell lines were designated as sensitive to 17-AAG if their survival was statistically significantly reduced compared to all of the WT cells. **D-H,**

Visualization of mono-cultured A549 and COR-L105 cells (**D**), H2023 and HCC827 cells (**E**), KYSE70 and KYSE30 cells (**F**), Huh-1 and Hep3B cells (**G**) and JHH5 and JHH2 cells (**H**), determined by total protein content, treated with 0.1% DMSO or the indicated concentrations of 17-AAG, for 8 days. Scale bar = 300 µm. **I,** Viabilities of mono-cultured ABC1 cells (with normal NRF2 regulation), determined by total protein content, exposed to the indicated concentrations of 17-AAG for 8 days, with and without co-treatment with the NRF2 inducer DEM (100 µM). **J,** Viabilities of mono-cultured KYSE30 cells (with normal NRF2 regulation), determined by total protein content, exposed to the indicated concentrations of 17-AAG for 8 days, with and without co-treatment with the NRF2 inducer DEM (100 µM). * $p < 0.05$.

Fig. 4 | Nrf2-dependent changes in the cellular phenotype are not required for the synthetic lethal effect.

A, The relative expression of the four HSP90 homologues in WT-GFP and Keap1 KO-mCherry cells as measured by qPCR. **B,** The relative expression of the Nrf2 target genes NQO1, GCLM and GSTM3 in response to 0.1% DMSO or 100 nM 17-AAG treatment for 24 hrs in WT-GFP and Keap1 KO-mCherry cells as measured by qPCR. **C,** The relative expression of the two βTrCP homologues BTRC and FBWX11, and the NRF2 target genes NQO1, HO1, GSTP1 and GCLM in A549 cells after treatment with an siRNA targeting βTrCP1/2, or a scrambled control, as measured by qPCR. **D,** The relative survival of A549 cells after 4 days of treatment with an siRNA targeting βTrCP1/2, or a scrambled control. Note that there is no change in cell survival upon hyperactivation of NRF2. **E,** The ratio of mCherry: GFP fluorescence from co-cultured WT-GFP and Keap1 KO-mCherry cells after 8 days treatment with either 0.1% DMSO or 100 nM 17-AAG, co-treated with the indicated concentrations of the antioxidant NAC. Note that 17-AAG kills the vast majority of Keap1 KO cells under all conditions, and therefore the ratio of mCherry: GFP is low in both the presence and absence of NAC. **F,** The ratio of mCherry: GFP fluorescence from co-cultured WT-GFP and Keap1 KO-mCherry cells after 8 days treatment with either 0.1% DMSO or 100 nM 17-AAG, cultured in media containing the indicated percentages of growth serum. **G,** Viabilities of co-cultured WT-GFP and Keap1-Nrf2 DKO-mCherry cells, determined by fluorescence intensity relative to the DMSO control, exposed to the indicated concentrations of 17-AAG for 8 days. **H,**

Visualization of the co-cultured WT-GFP and Keap1-Nrf2 DKO-mCherry cells shows that in co-cultures treated with 800 nM 17-AAG, the mCherry signal from the DKO cells dominates the surface of the microplate well. Scale bar = 300 µm. **I,** Viabilities of co-cultured WT-GFP and Keap1 KO-mCherry cells, determined by fluorescence intensity, exposed to combinations of 0.1% DMSO, 100 nM 17-AAG and 2 µM Kribb11 (HSF1 inhibitor). * $p < 0.05$. **J,** Relative cell death of A549 and COR-L105 cells exposed to 0.1% DMSO or 200 nM 17-AAG for 3 days, as determined using the CellTox membrane permeability assay.

Fig. 5 | The geldanamycin scaffold is required for the synthetic lethal interaction with NRF2.

A, Chemical structures of the HSP90 inhibitors 17-AAG, 17-DMAG, PU-H71, Radicicol, NVP-BEP800 and BIIB021. **B-F.** Viabilities of mono-cultured A549 (orange line) and COR-L105 cells (blue line), determined by total protein content, exposed to the indicated concentrations of 17-DMAG, PU-H71, Radicicol, NVP-BEP800 and BIIB021 for 8 days. **G,** Visualization of mono-cultured A549 and COR-L105 cells, treated with 0.1% DMSO or 50 nM 17-DMAG, for 8 days. Scale bar = 300 µm. **H,** Viabilities of co-cultured WT-GFP and Keap1 KO-mCherry cells, determined by fluorescence intensity, exposed to the indicated concentrations of 17-DMAG for 8 days. **I,** Visualization of the co-cultured WT-GFP and Keap1 KO-mCherry cells shows that in response to DMSO, the co-culture is dominated by mCherry expressing cells, while in 17-DMAG treated cells, the mCherry signal is significantly diminished, and the GFP expressing cells expand their domain to fill the entire surface of the microplate well. Scale bar = 300 µm **J, K,** Viabilities of co-cultured WT-GFP and Keap1 KO-mCherry cells, determined by fluorescence intensity, exposed to the indicated concentrations of NVP-BEP800 and PU-H71 for 8 days.

Fig. 6 | Geldanamycin-derived IPI-504 is synthetic lethal with NRF2.

A, Viabilities of mono-cultured A549 (orange line) and COR-L105 cells (blue line), determined by total protein content, exposed to the indicated concentrations of IPI-504 for 8 days. **B,** Visualization of mono-cultured A549 and COR-L105 cells, treated with 0.1% DMSO or 100 nM IPI-504, for 8 days. Scale bar = 300 µm. Note that only the A549 cells displayed toxicity towards 100 nM IPI-504. **C,** Viabilities of mono-cultured Huh-1 and Hep3B cells, determined by total protein content, exposed to the indicated concentrations of IPI-504 for

8 days. **D,** Visualization of mono-cultured Huh-1 and Hep3B cells, treated with 0.1% DMSO or 100 nM IPI-504, for 8 days. Scale bar = 300 µm. **E,** Viabilities of co-cultured WT-GFP and Keap1 KO-mCherry cells, determined by fluorescence intensity, exposed to the indicated concentrations of IPI-504 for 8 days. **F,** Visualization of the co-cultured WT-GFP and Keap1 KO-mCherry cells shows that in response to DMSO, the co-culture is dominated by mCherry expressing cells, while in response to increasing concentration of IPI-504, the mCherry signal significantly diminishes, while the GFP expressing cells expand their domain to fill the entire surface of the microplate well. Scale bar = 300 µm

Fig. 7 | Metabolism of 17-AAG to 17-AAGH$_2$ by the NRF2 target gene NQO1 provides the specificity for the synthetic lethal interaction.

A, Structure of the geldanamycin drug scaffold, with the location of the quinone groups highlighted with an asterisk. **B,** Concentrations of the 17-AAG metabolite 17-AAGH$_2$ analysed using LC-MS, and calculated based on the peak area detected at 4.9 min on the chromatograms, from samples collected from WT-GFP and Keap1 KO-mCherry cells exposed to the indicated concentrations of 17-AAG for 24 hrs. * $p < 0.05$, ** $p < 0.005$. **C,** The relative expression of the NRF2 target genes NQO1 and TXNRD1 from a range of human cancer cell lines as measured by qPCR. Cells with aberrant NRF2 activation are shown in black, while those with normal NRF2 regulation are shown in white. **D,** Viabilities of mono-cultured A549 and COR-L105 cells, determined by total protein content, exposed to the indicated concentrations of β-lapachone for 8 days. Note that, while β-lapachone is also a substrate for NQO1, A549 cells show decreased toxicity to β-lapachone. This is in sharp contrast to the toxicity profile of 17-AAG, suggesting that the synthetic lethal relationship between NRF2 and 17-AAG does not extend to all NQO1 substrates. **E,** Viabilities of mono-cultured A549, determined by total protein content, exposed to the indicated concentrations of 17-AAG, co-treated the NQO1 inhibitor dicoumarol (10 µM) and/ or the TXNRD1 inhibitor auranofin (50 nM), for 4 days. * $p < 0.05$. **F,** Immunoblot showing the NQO1 status of four different Huh-1 CRISPR-Cas9 generated clones. Only clone #6 is a knockout. **G,** Relative cell survival of Huh-1 cells, determined by total protein content, exposed to the indicated concentrations of 17-AAG for 8 days, and co-treated with the TXNRD1 inhibitor auranofin, AUR (100 nM), or compared to the isogenic NQO1 KO cell line generated using CRISPR-Cas9.

Fig. 8 | 17-AAG displays activity against NRF2-dependent tumours *in vivo*, and, when used in combination with AKT inhibition.

A, Representative IVIS images of *in vivo* mCherry expression from Keap1-mCherry Hepa1 cells transplanted into Nude mice. The mice were treated with either vehicle or 100 mg/kg 17-AAG three times per week for 3 weeks. **B,** Fold change in tumour size determined by *in vivo* mCherry expression over the 21-day 17-AAG treatment period shown in **a**. N = 5 mice per group. * $p < 0.05$**. C,** Over the 21-day experimental period, treatment with 100 mg/kg 17-AAG had no impact on mouse body weight changes relative to the vehicle control. **D,** Viabilities of mono-cultured A549 and COR-L105 cells, determined by total protein content, exposed to the indicated concentrations of the AKT inhibitor MK2206, with or without 100 nM 17-AAG, for 8 days. Note that only the A549 cells displayed increased toxicity towards MK-2206 when co-treated with 100 nM 17-AAG. **E,** Viabilities of mono-cultured Huh-1 and Hep3B cells, determined by total protein content, exposed to the indicated concentrations of the AKT inhibitor MK2206, with or without 100 nM 17-AAG, for 8 days. **F,** Viabilities of mono-cultured Huh-1 and Hep3B cells, determined by total protein content, exposed to the indicated concentrations of paclitaxel, with or without 200 nM 17-AAG, for 8 days.

Fig. 9| The mechanism through which 17-AAG is synthetic lethal with NRF2 activity.

Summary showing the mechanism through which 17-AAG displays synthetic lethality with NRF2. In NRF2-activated tumours, high levels of NRF2 result in increased cytoprotective enzyme gene expression, particularly NQO1. For a given concentration of 17-AAG, the higher levels of NRF2 target gene expression result in a significant increase in the generation of the 17-AAG metabolite 17-AAGH_2, which results in enhanced HSP90 inhibition and cell death.

Figure 1

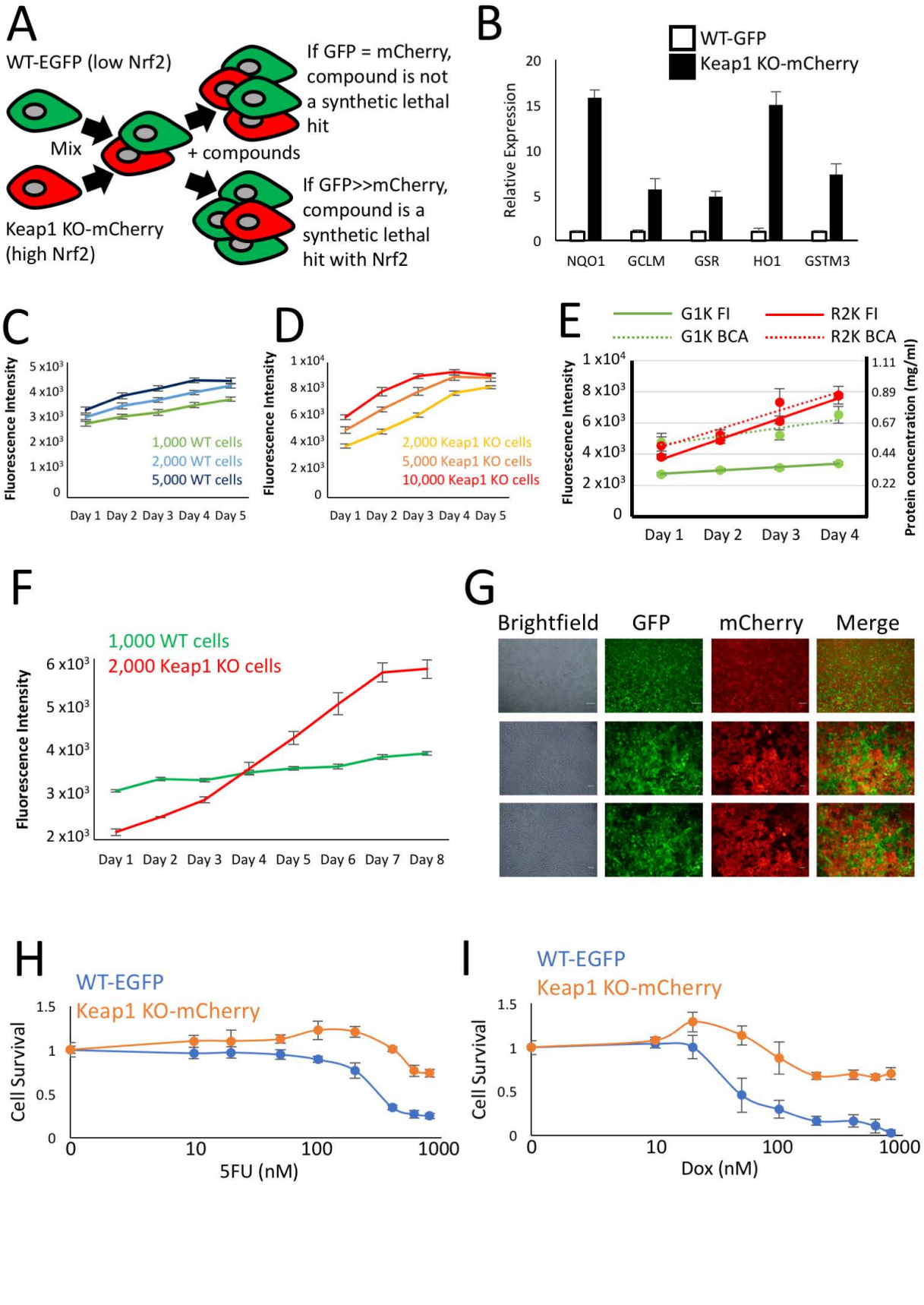

Figure 2

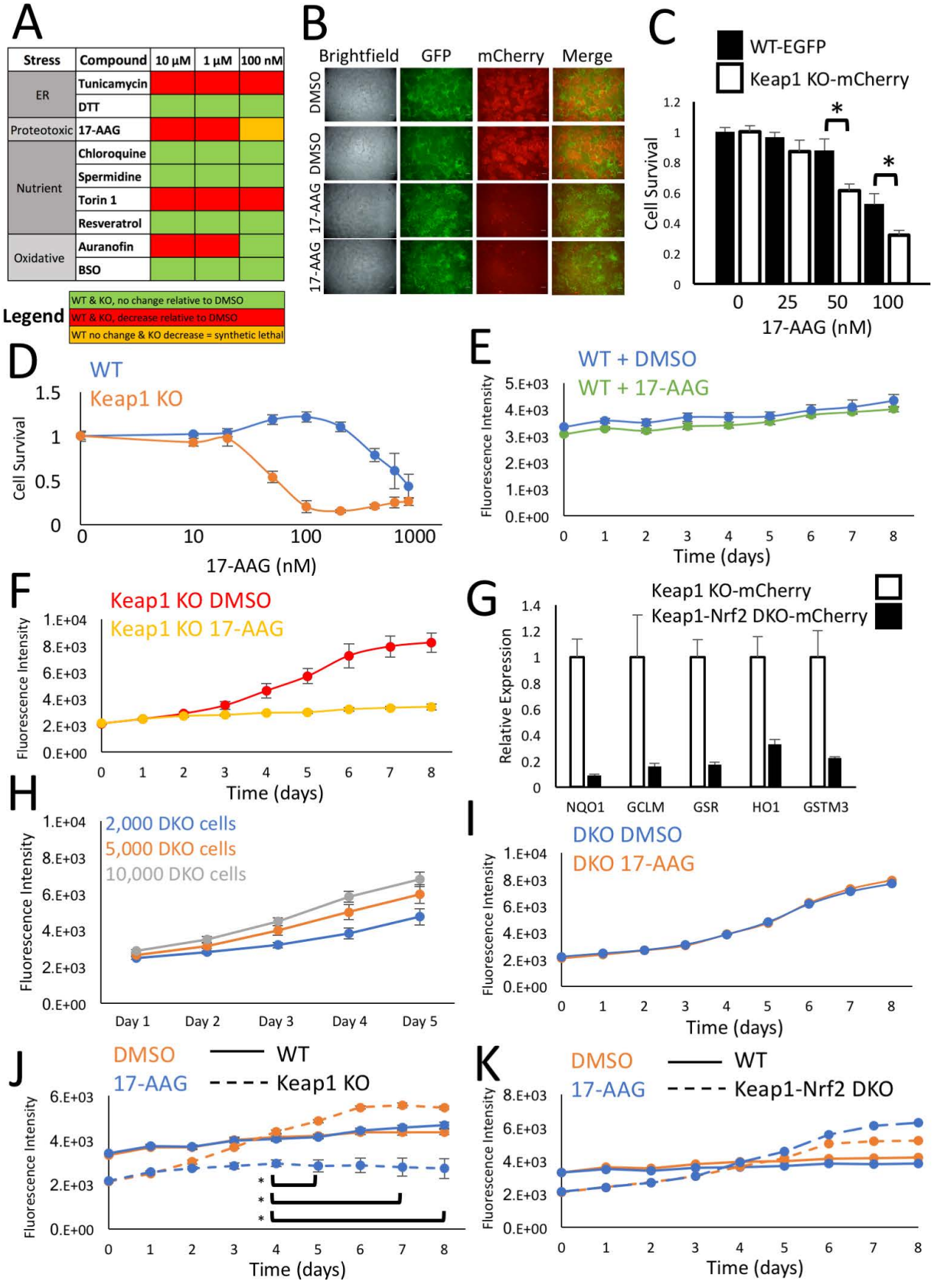

Figure 3

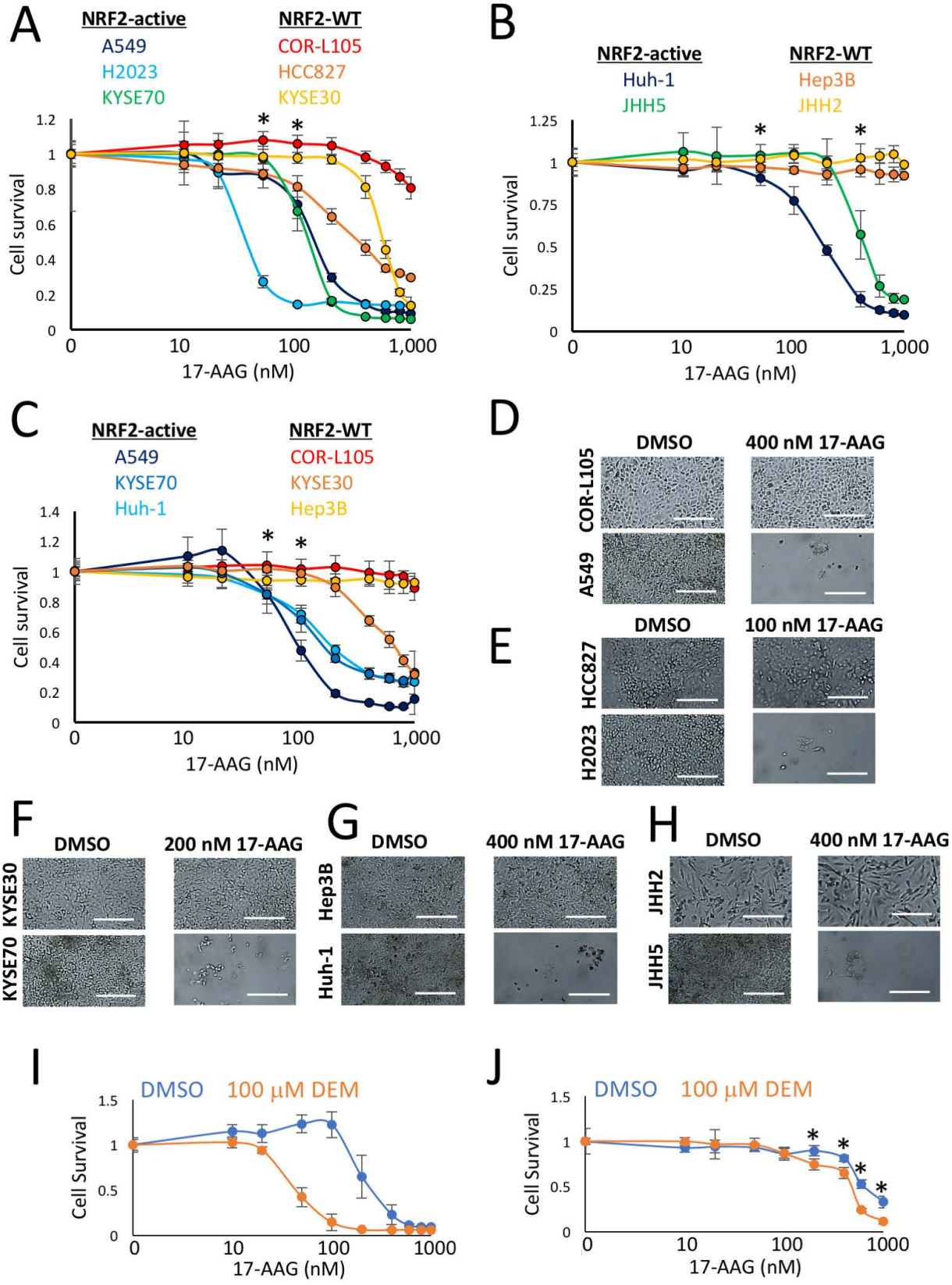

Figure 4

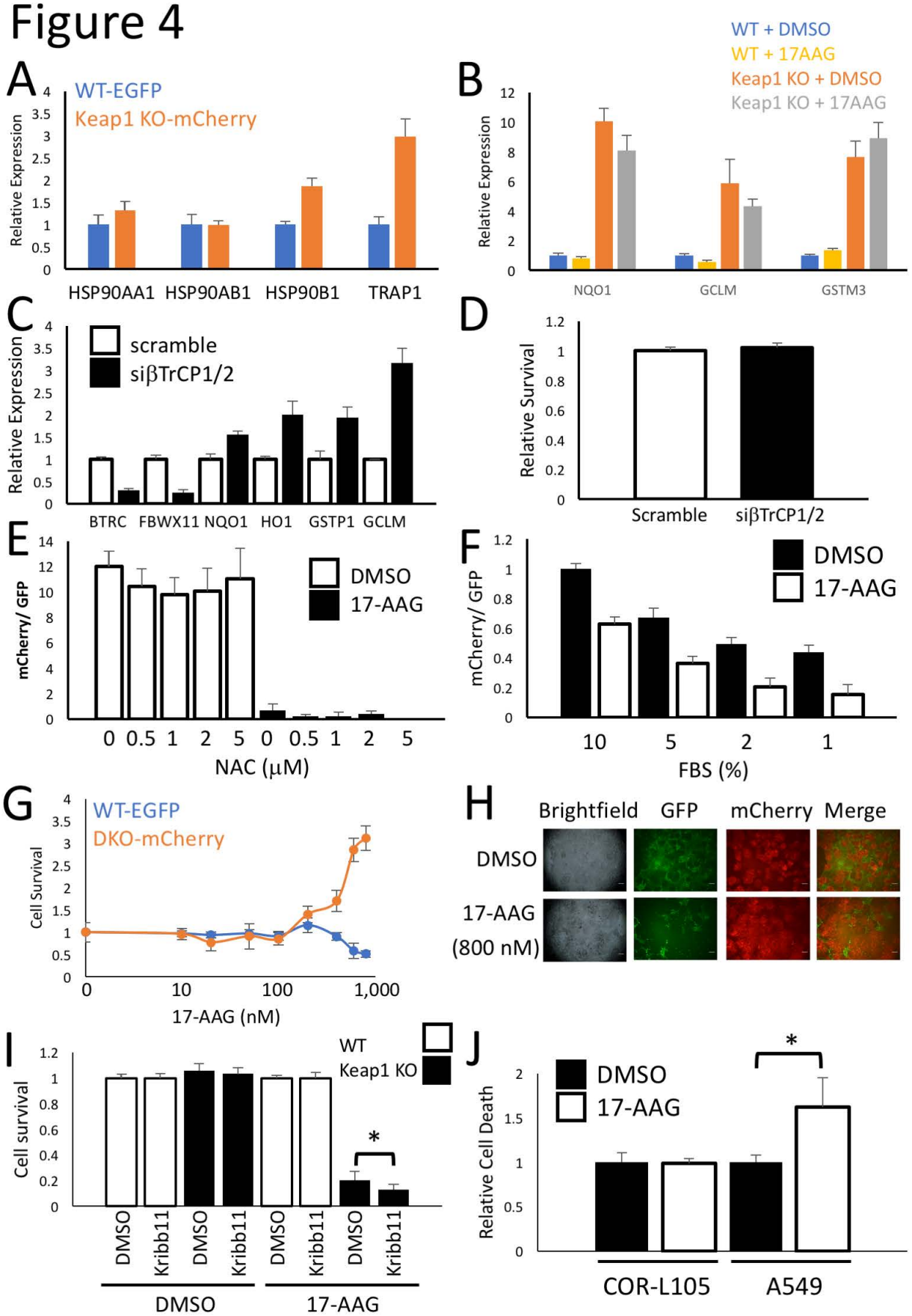

Figure 5

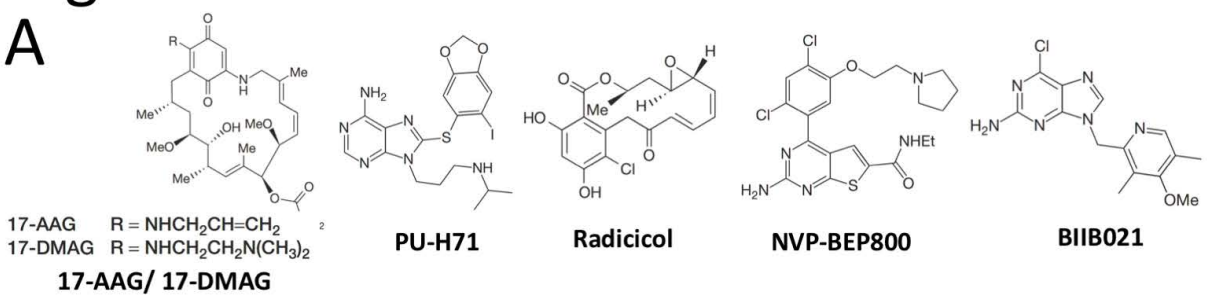

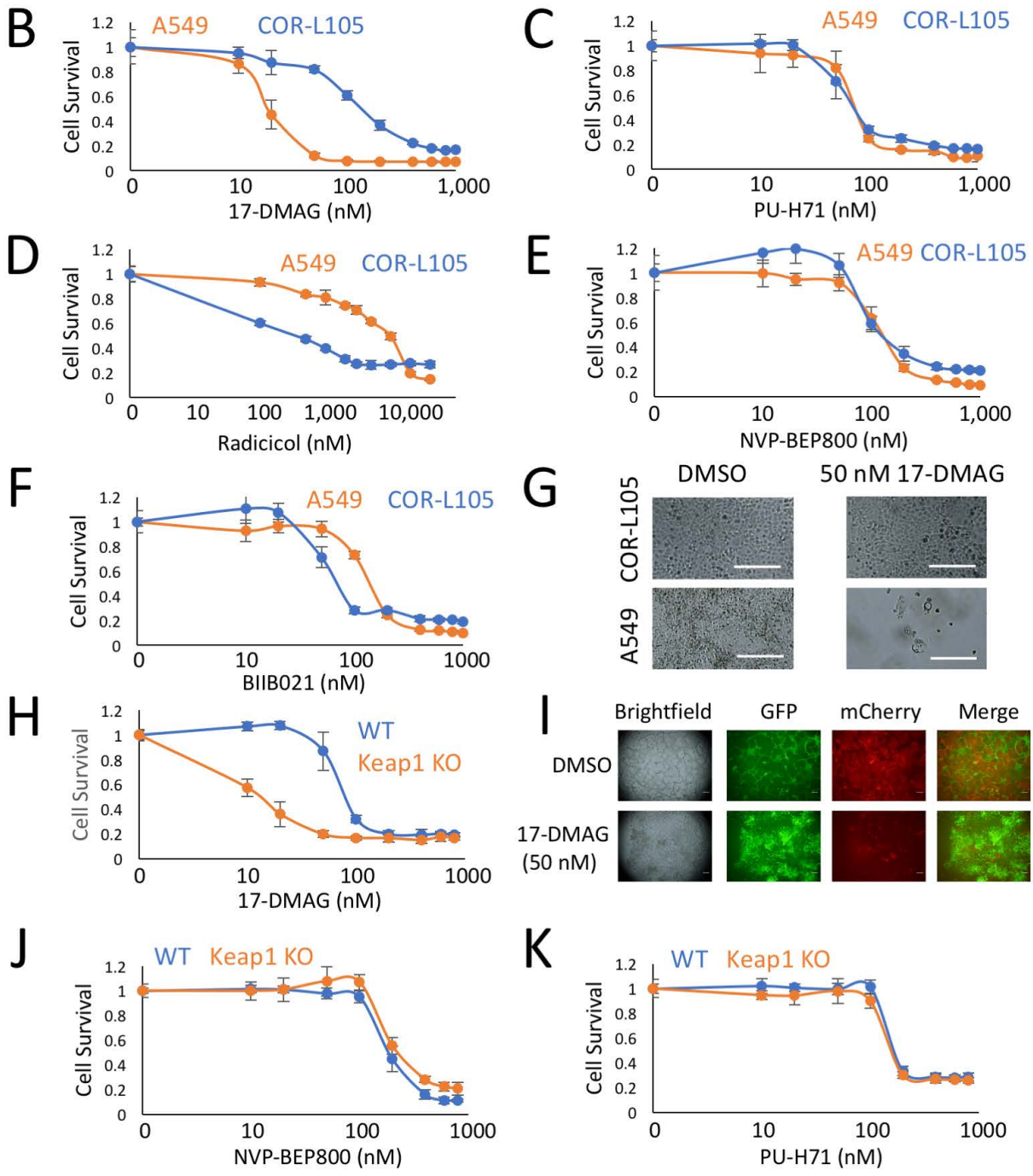

Figure 6

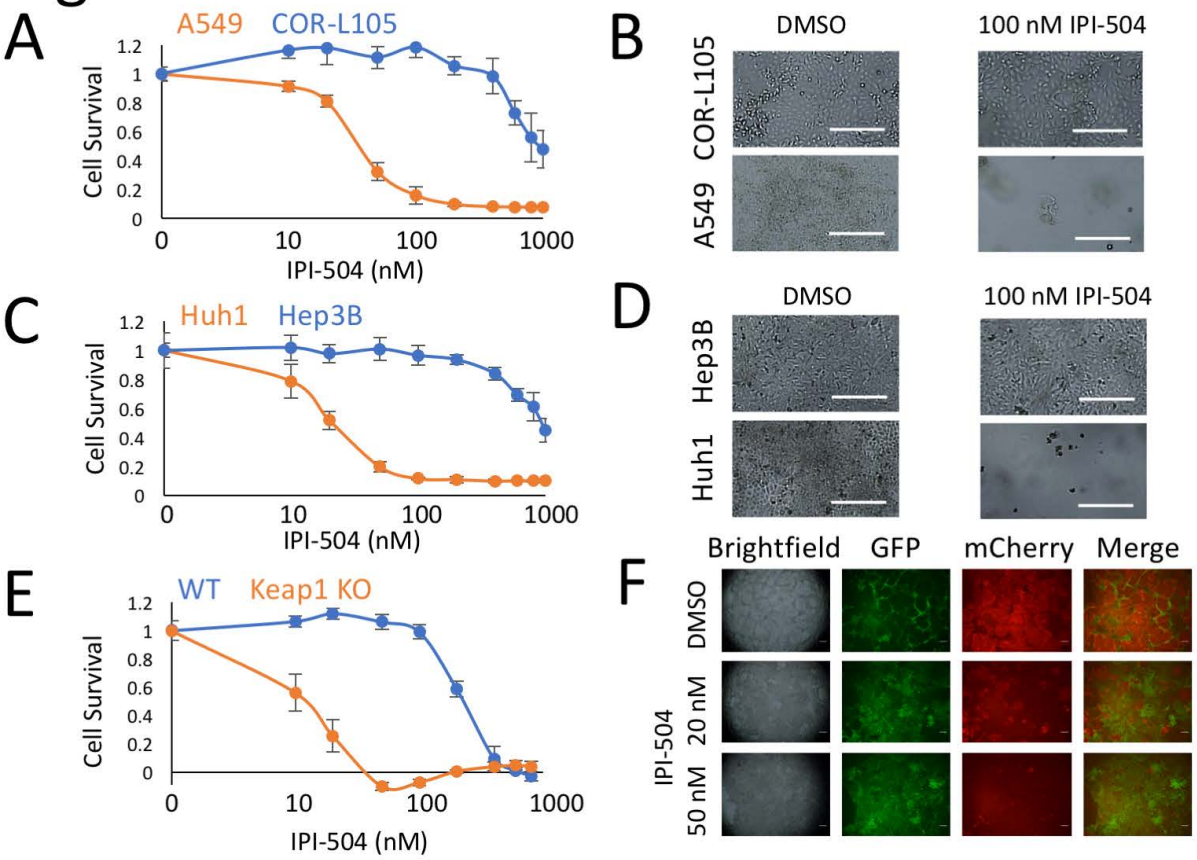

Figure 7

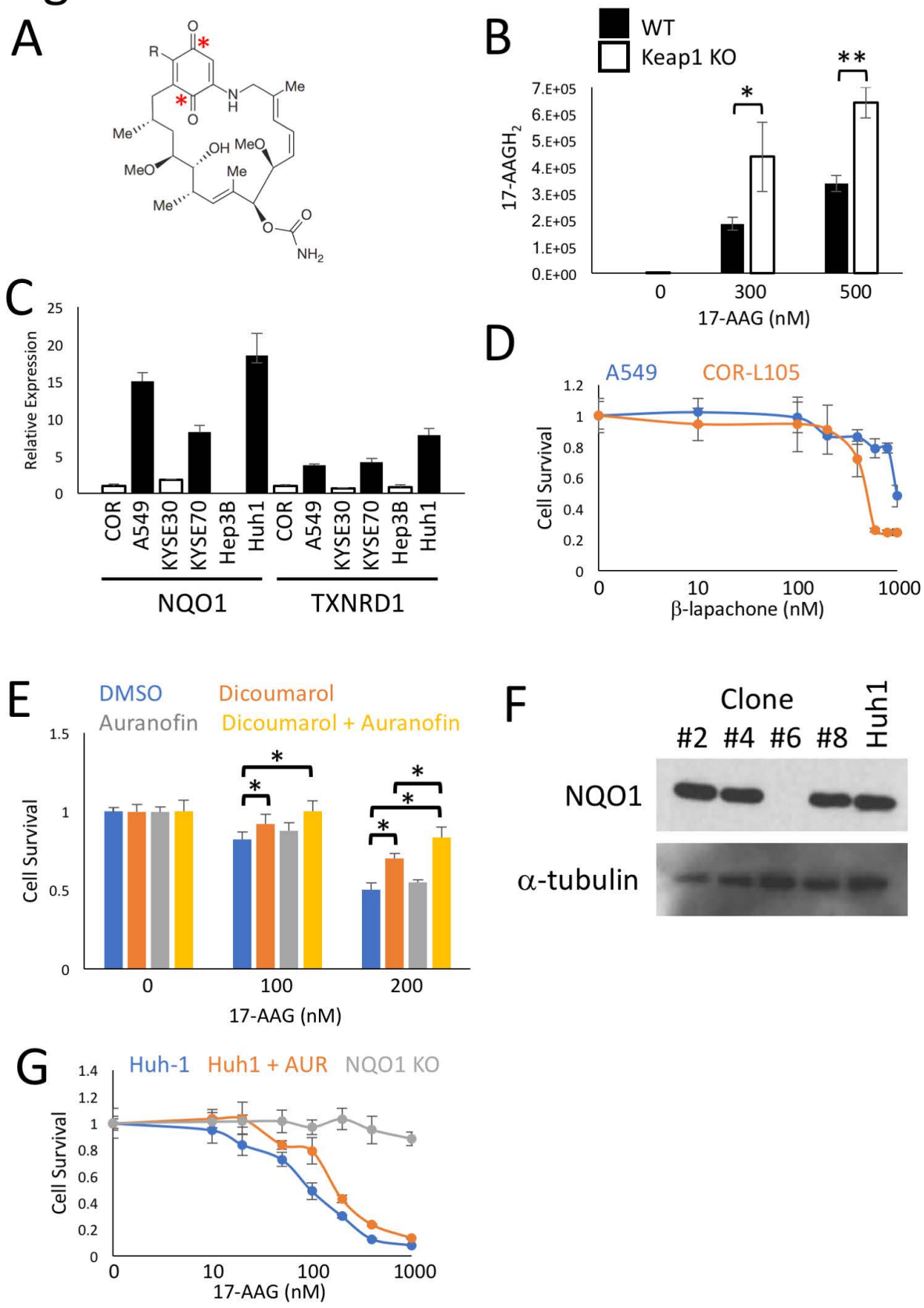

Figure 8

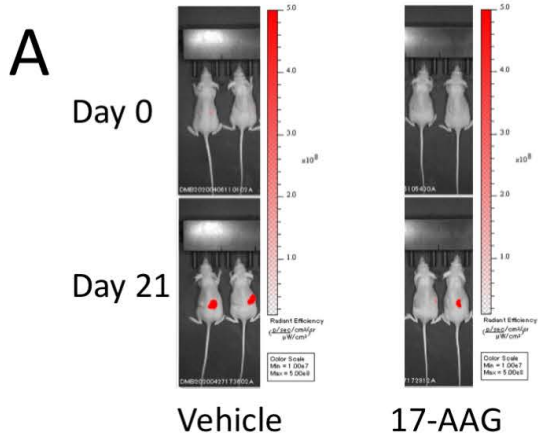

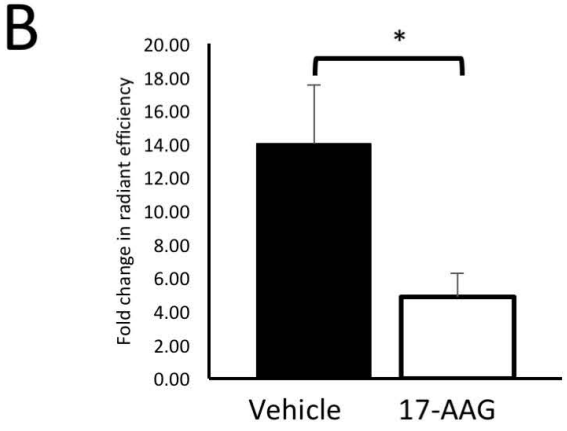

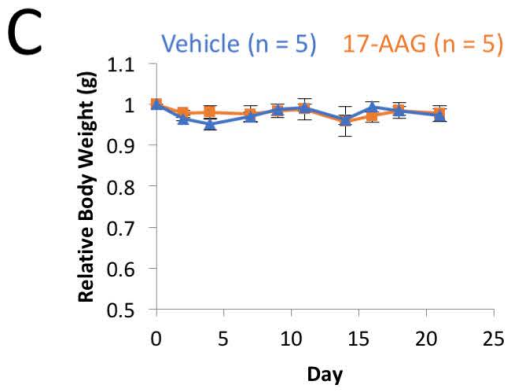

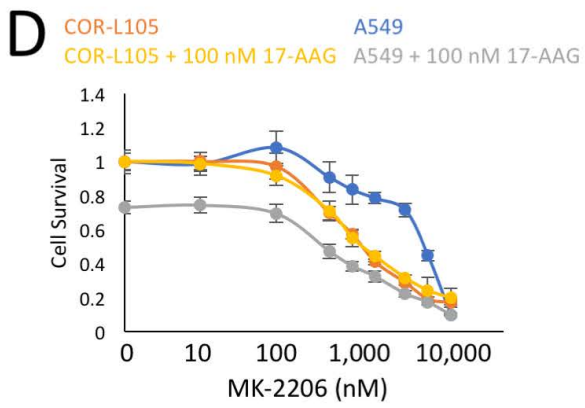

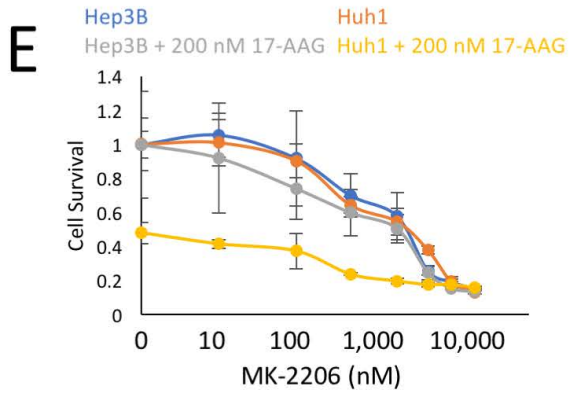

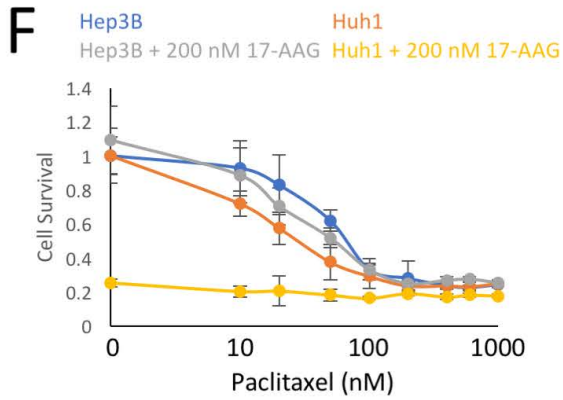

Molecular and Cellular Biology

Figure 9